mater.scichina.com link.springer.com

Published online 19 February 2024 | https://doi.org/10.1007/s40843-023-2665-8
Sci China Mater 2024, 67(4): 1014–1041

SPECIAL TOPIC: Computation-assisted Materials Screening and Design

Progress in the prognosis of battery degradation and estimation of battery states

Jun Yuan[1,2†], Zhili Qin[2,3†], Haikun Huang[1,2], Xingdong Gan[1,2], Ziwei Wang[4], Yichen Yang[4], Shujiang Liu[1,2], An Wen[2], Chuang Bi[2], Baihai Li[1,2*] and Chenghua Sun[5*]

ABSTRACT **Lithium-ion batteries (LIBs) have gained immense popularity as a power source in various applications. Accurately predicting the health status of these batteries is crucial for optimizing their performance, minimizing operating expenses, and preventing failures. In this paper, we present a comprehensive review of the latest developments in predicting the state of charge (SOC), state of health (SOH), and remaining useful life (RUL) of LIBs, and particularly focus on machine learning techniques. This paper delves into the degradation mechanisms of LIBs and their underlying theories, providing an in-depth analysis of the strengths and limitations of various machine learning techniques used to predict SOC, SOH and RUL. Furthermore, this review sheds light on the challenges encountered in the practical application of electric vehicles, especially concerning battery degradation. It also offers valuable insights into the future research directions for LIBs. While machine learning methods hold great promise in enhancing the accuracy of predicting SOC, SOH, and RUL, there remain numerous technical and practical obstacles that must be overcome to make them more applicable in real-world scenarios.**

Keywords: state of charge, state of health, remaining useful life, lithium-ion batteries, equivalent-circuit model, electrochemical model, machine learning

INTRODUCTION

The escalating environmental pollution and the limited supply of fossil fuels have spurred a rising interest in clean and renewable energy sources. The development of new-energy electric vehicles (EVs) as a substitute for traditional vehicles has been a major focus in this regard [1–3]. With the rapid increase in the production of new energy EVs, the number of retired batteries is also rapidly increasing, given the limited lifespan of batteries. Consequently, addressing the issues related to batteries has become an urgent challenge that needs to be tackled [4].

EVs batteries can be categorized into three types based on their capacity and output power: energy/power-balanced, power-type, and energy-type batteries. The power battery serves as a substitute for fuel [5] and plays a crucial role in determining the safety, efficiency, economy, and service life of the EV, directly impacting the performance of EVs. Out of the various types of batteries available, Lithium-ion batteries (LIBs) have emerged as the predominant devices to power new energy vehicles owing to their high energy density, extended service life, cost-effectiveness, and eco-friendliness [6,7]. Moreover, LIBs exhibit no memory effect and offer a voltage output nearly three times that of NiCd batteries, thereby minimizing the need for additional batteries and accompanying hardware [8]. As the core component of EVs, LIBs are a vital factor in determining the overall value of an EV. Hence, the health management, security early alarm, performance optimization, and utilization of LIBs have become crucial areas of research [9]. Commercial LIBs commonly employ $LiFePO_4$, $Li(Ni_xCo_yMn_z)O_2$, $LiMn_2O_4$, $LiNiO_2$, or $LiCoO_2$ as cathodes and $Li_4Ti_5O_{12}$ or graphite as anodes, while electrolyte salts such as $LiPF_6$, $LiBF_4$, $LiClO_4$, ethylene carbon, or diethyl carbonate are used [8–10]. Due to the poor thermal stability, $LiMn_2O_4$ and $LiCoO_2$ batteries are seldom used in commercial EVs. On the contrary, commercialized $LiFePO_4$ batteries exhibit excellent durability and cycle stability. Ternary batteries $Li(Ni_xCo_yMn_z)O_2$ has a higher discharge voltage platform, higher energy density and specific capacity. The energy density of ternary battery cells and modules exceeds 200 W h kg^{-1}, which is higher than that of $LiFePO_4$ batteries (approximately 136 W h kg^{-1}). As a result, ternary batteries can provide EVs with longer driving range. Both $LiFePO_4$ batteries and ternary batteries demonstrate excellent discharge performance under high-rate conditions.

In practical applications, performance durability has been a target since the first commercial LIBs. However, achieving this target has been quite challenging as the electrochemical composition continuously degrades during charging/discharging cycles. Notable examples of this degradation include the decrement of lithium-ion concentration and the rapid formation of complicated impurity phases at the electrode-electrolyte inter-

[1] School of Materials and Energy, University of Electronic Science and Technology of China, Chengdu 611731, China
[2] Yangtze Delta Region Institute (Huzhou), University of Electronic Science and Technology of China, Huzhou 313001, China
[3] School of Computer Science and Engineering, University of Electronic Science and Technology of China, Chengdu 611731, China
[4] Power Research Institute of State Grid Shaanxi Electric Power Company Limited, Xi'an 710100, China
[5] Department of Chemistry and Biotechnology, Swinburne University of Technology, Hawthorn, Victoria 3122, Australia
[†] These authors contributed equally to this work.
[*] Corresponding authors (emails: libaihai@uestc.edu.cn (Li B); chenghuasun@swin.edu.au (Sun C))

 © Science China Press 2024

face, leading to a significant increase in internal resistance (IR). Under such circumstances, the capacity and usable power gradually decrease, a phenomenon referred to as battery aging [11,12], and battery aging occurs in two patterns: calendar and cycle aging [13,14]. Calendar aging mainly relates to the unavoidable capacity fade during the battery storage process, and it has a strong sequential relationship with time. As demonstrated, both the temperature and state of charge (SOC) directly affect the calendar aging of the battery [15]. Cyclic aging is a battery aging phenomenon that is affected by various parameters of the battery's usage cycle, such as the number of charges/discharge cycles, usage pattern, charge and discharge rate, operating environment, temperature and thermal stress. Since battery aging is influenced by several factors, predicting battery health and lifetime has become a popular and challenging research topic [16,17].

In principle, the battery should be considered at the end of its useful life when its capacity falls below 80% of the initial capacity or its IR exceeds twice the initial resistance [18–20]. Battery aging is a highly complex process, with numerous factors contributing to the degradation of LIBs performance, including physical factors such as mechanical stress and thermal stress due to temperature changes, as well as chemical factors such as electrochemical reactions during the charging and discharging process. Various aging processes, changes in equipment conditions, and dynamic operating environments lead to nonlinear and uncertain performance degradation [21]. Therefore, accurate estimation of battery health status and remaining useful life (RUL) is critical for early detection of battery performance issues, system maintenance, safe production, and secondary recycling. To achieve this, appropriate and accurate battery health metrics and prognostic methods are required [22].

Currently, the state of health (SOH), SOC, and RUL are the three main indicators of battery status, which can be determined by measuring internal IR, capacitance, power, and other aging characterization factors. The ratio of the battery's maximum available capacity to its nominal capacity is a common quantitative criterion used to determine SOH. SOC refers to the ratio of the remaining capacity of the battery to its maximum available capacity. Accurate estimation of SOH and SOC ensures the safety and reliability of battery systems, and provides the foundation for energy safety management [3]. Furthermore, RUL is defined as the time or number of cycles at which the device performance first falls below a failure threshold [23,24].

Accurately predicting the RUL of a battery can be immensely beneficial for battery recycling and cascade utilization. It can help maximize the potential of the battery and extend its service life before it requires replacement and disposal. As mentioned earlier, parameters such as SOH, SOC, and RUL are indicators of the battery's aging state, which have been extensively measured or calculated using various approaches [24–26]. Currently, the SOC and SOH of a battery can be determined to some extent using an advanced battery management system (BMS). However, the BMS has limitations in terms of estimation accuracy. The battery's static capacity, which is obtained through a maximum-capacity test, is a vital parameter for SOH and SOC calculations, but it does not reflect the state under actual dynamic conditions in real-time, which delays the battery's health estimation. Although other metrics, such as state of function (SOF), state of energy (SOE), and state of power (SOP) [27], can be used to evaluate battery performance, research on these metrics has been relatively limited. Overall, accurate estimation of SOC, SOH, and RUL indicators has been a challenging area of research in recent years.

This paper provides a review of the fundamental mechanisms and theories of LIBs and summarizes the commonly used methods for estimating SOH, SOC, and RUL, with a particular focus on various data-based approaches, followed by a perspective regarding their advantages and disadvantages. Our objective is to provide theoretical knowledge on LIBs that can be useful for both research and commercial technology development. We hope that this review will facilitate the study and advancement of LIBs health management and prognostication.

The review is structured as follows: we first present an overview of the paper and introduce the key definitions to establish a foundation for subsequent sections. In the section of "AGING MECHANISMS AND INFLUENCING FACTORS", we discuss the aging mechanisms and commonly studied factors based on the charging/discharging principle and structure of LIBs, and provide the basis for subsequent estimation of SOC, SOH, and RUL. In the section of "TRADITIONAL TECHNOLOGIES FOR SOC, SOH AND RUL ESTIMATION", we review various traditional technologies for predicting a battery's SOC, SOH and RUL, and discuss their merits and drawbacks. In the section of "MACHINE LEARNING METHODS FOR SOC, SOH AND RUL ESTIMATION", we provide an in-depth description of data-based methods, with a particular focus on various machine learning techniques, and offer a detailed explanation of algorithms based on auto-regression, artificial intelligence (AI) networks, support vector machines, etc.

AGING MECHANISM AND INFLUENCING FACTORS

Battery aging is an inevitable process that leads to a reduction in the capacity and power of batteries over time. This degradation not only shortens the service life of the batteries but can also pose a safety risk. Scientists have diligently investigated the complex physical and chemical reactions within LIBs over the last few decades, and various aging mechanisms within the batteries have been identified thanks to the advent of more accurate electrochemical analysis equipment. For example, Wang *et al.* [28] investigated the reaction kinetics between LiOH and I_2 by combining calculations and machine learning technology, and further explored the influence of the degree of disorder of LiOH and the solvents effects.

Taking the cubic Li-argyrodites as an example, Zhao *et al.* [29] identified the conduction of Li^+ by constructing a generic technique of hierarchically encoding crystal structure (HECS). Based on these observations, it has been demonstrated that the aging mechanism actually varies greatly depending on many factors, such as the type of battery and external factors [30,31]. Although electrode materials in batteries can vary greatly, common patterns for battery degradation have been identified, including loss of Li-ion inventory (LLI), loss of active materials (LAM), and IR increase [32,33]. This section reviews battery degradation on cathode and anode materials, outlines the aging mechanisms and side reactions, and further analyzes the key factors that contribute to performance degradation.

Aging mechanism

Battery degradation mechanism

Within a battery, electrochemical processes occur as the number

 © Science China Press 2024

of cycles increases, and they are often accompanied by a series of irreversible side reactions (aging reactions) [14,34]. As shown in Fig. 1, battery charging/discharging cycles are realized by embedding and detaching lithium ions between the positive and negative electrodes. During the charging process, the external circuit current flows from the negative electrode to the positive one; within the battery, the negative electrode receives electrons (reduction) while the positive electrode releases them (oxidation), simultaneously. Lithium ions separate from the positive electrode, pass through the polymer diaphragm layer, enter the electrolyte, and finally embed in the negative electrode. Battery discharge is a reverse process, and a series of factors during repeated charging/discharging process will lead to the battery aging, such as the formation of solid electrolyte on the electrode and electrolyte surface, the deposition and depletion of lithium ions, the dissolution of the active material and electrolyte, the destruction of the electrode structure, and the phase change of the electrode material [35].

Essentially, battery degradation is influenced by the basic components (electrodes, electrolyte and membranes) and major electrochemical reactions [36]. As shown in Fig. 2, the battery's capacity is primarily determined by the quantities of active material and available lithium ions. Among various battery degradation modes, the LLI is mainly caused by processes such as the formation and decomposition of the solid electrolyte interface (SEI) film, the formation of lithium plating layer material, electrolyte decomposition, and other related processes that lead to a reduction in available lithium-ions. Additionally, low temperatures, fast charging, and overcharging can also contribute to electrolyte decomposition and lithium ions precipitation [37]. LAM is caused primarily by joint agent decomposition, collector corrosion, loss of electrical contact, and cracking of electrode particles due to peeling of the graphite layer [38]. In the literature, LAM aging mechanism is subdivided into the loss of lithiated/delithated cathode and anode materials [30,39]. Battery degradation modes also include an increase of IR and loss of electrolyte. Significant electrolyte loss primarily affects the concentration of active material, additives and lithium ions in the electrolyte, resulting in the LAM and a reduced battery capacity.

Aging mechanism of anode materials

Currently, graphite anode is the dominating one. However, lithium ions are theoretically unstable on the graphite surface because the working voltage of the graphite anode falls outside the voltage stablization window of the electrolytes. Specifically, the working voltage of the graphite anode is around 0.05 V, whereas the conventional liquid organic electrolyte is electrochemically stable within a range of approximately 1–4.5 V [40]. As a result, particularly during the first cycle of the initial charging process, the formation of a passivation protective layer known as SEI occurs easily, which is mainly made up of electrolyte decomposition products generated on the graphite electrode, resulting in the partial loss of battery capacity [41]. The formation of SEI is heavily influenced by the specific composition and structure of the carbon electrodes, which includes factors such as particle size, pore size, crystallinity, chemical impurities, and the ratio of basal to edge planes. During the observation of electrode structures during the discharge process, Barré *et al.* [35] demonstrated that the morphology of the positive electrode did not change significantly in batteries with different levels of utilization, which indirectly confirms the central role that the negative electrode plays in battery aging. Specifically, the impact of SEI on batteries is mainly due to the volume changes associated with lithium-ion intercalation and delamination processes in graphite electrodes, which result in a depletion of lithium-ion stock and an increase in IR, ultimately leading to a decrease in capacity density. The continuous growth

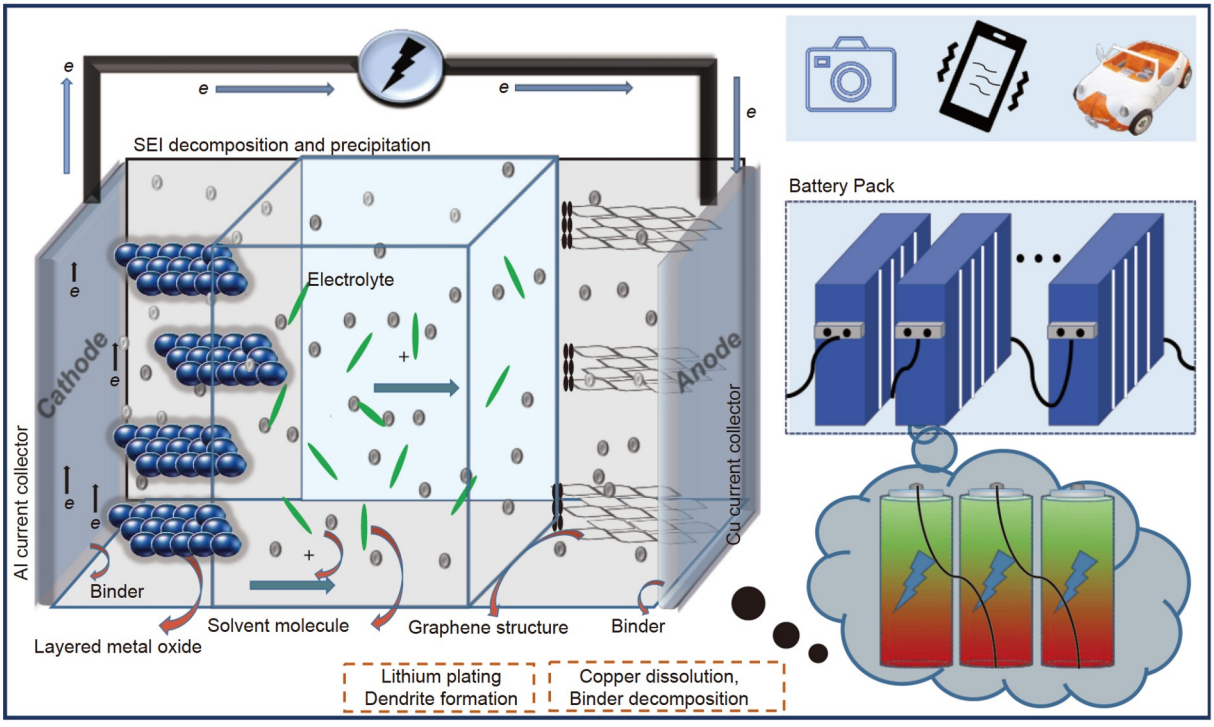

Figure 1 Framework about the charging process of LIB.

© Science China Press 2024

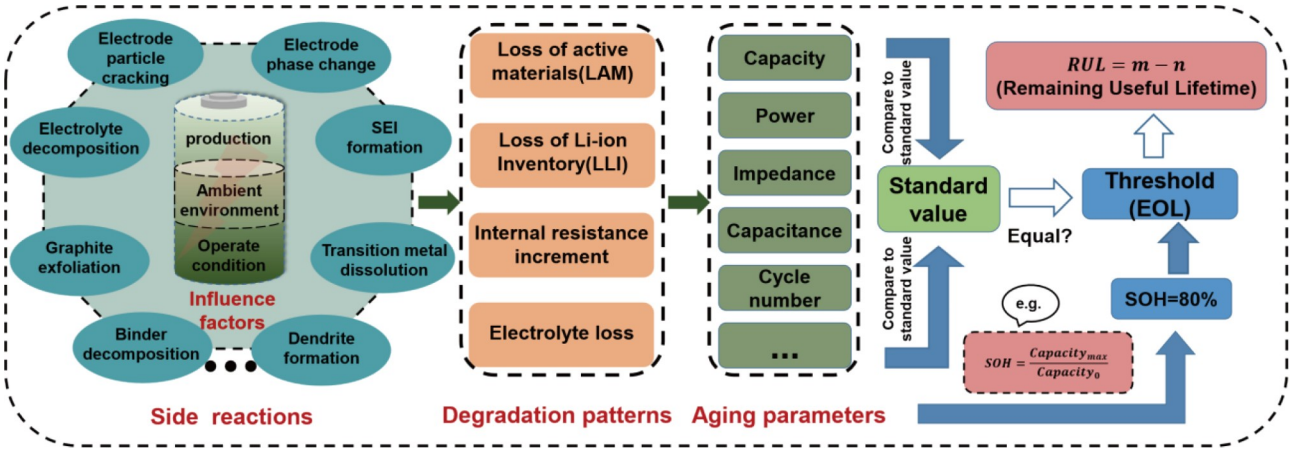

Figure 2 Influencing factors and degradation mechanism of battery aging.

of SEI has been identified as the primary cause of LIBs aging [13,42]. Interestingly, when in good condition, SEI can also play a positive role by providing good insulation, excellent lithium ions conductivity, and lower electron conductivity. These properties can promote ion insertion, reduce stress during the electrochemical reaction, and adapt to changes in anode volume [43,44].

Besides graphite electrodes, spinel lithium titanium oxide (LTO) and silicon-based anodes are also commonly used. LTO is a zero-strain material that does not undergo any volume changes during the intercalation and deintercalation of lithium ions. Furthermore, LTO has a longer lifespan because its potential remains within the stable range of the electrolyte, preventing the generation of SEI film. Additionally, the relatively high voltage also prevents the reduction of lithium ions and the dissolution of metal materials [45,46]. Compared with LTO, silicon-based anode operates outside the electrolyte-stabilized voltage window. Consequently, SEI film readily forms, which can even cause electrode cracking due to the severe volume expansion. Despite this drawback, the silicon-based anode has been rapidly developed due to its low cost and high specific capacity. In practice, pure silicon is generally not utilized as an anode material due to conductivity and power concerns. Instead, a carbon/silicon compound is commonly employed to enhance capacity utilization and prolong battery life [47].

Aging mechanism of cathode materials

The primary degradation mode differs for various cathode materials. The formation of solid electrolytes on the electrode surface, electrolyte decomposition, and lithium plating contribute to the depletion of the lithium-ion inventory during cycles. Furthermore, changes in the volume of the active material, decomposition and dissolution of chemical substances, can lead to degradation of the electrode structure and the formation of a parasitic phase, which in turn can increase the IR of the battery and reduce its performance. During the discharge process, lithium ions diffuse more rapidly in the electrolyte than cathode particles due to their smaller size. This enables them to more easily reach the negative electrode and be adsorbed onto its surface or inserted into the cathode material. For instance, the commonly used LMO spinel cathode material may experience a Jahn–Teller distortion due to the insertion of extra lithium ions. This can cause the material to transform from cubic to tetragonal phase, resulting in a volume change [48,49]. Moreover, because of the highly reactive nature of lithium ions, they are susceptible to reacting with the cathode material particles, forming insoluble compounds that can increase the IR of the battery [50]. Furthermore, cathode materials may dissolve into the electrolyte, which is often accompanied by the migration of the dissolution substance and the precipitation reaction on the anode, accelerating SEI formation [14].

Factors affecting battery performance

Under the operation condition, battery performance can be affected by various factors, including the temperature, over-charge/over-discharge, mechanical stress, and charge/discharge rate. Temperature is one of the most important factors affecting battery life because it directly affects the severity of internal side reactions. It is worth noting that battery temperature can be affected by various factors such as operating temperature, heating and cooling systems, battery heat capacity, thermal conductivity, and battery heat generation. Typically, battery aging increases when the temperature drops below 25°C due to the rapid plating of lithium ions on battery anodes, leading to irreversible lithium ion depletion and hindered insertion [51]. When the temperature is too low, the transfer of lithium ions slows down significantly, resulting in severe blockage during the transfer process, ultimately leading to localized lithium transition and dendrite formation [52]. However, if the temperature exceeds 25°C, it can also accelerate battery aging [53]. High temperatures can accelerate the formation of SEI and rapidly increase the IR of the battery. Additionally, elevated temperatures can lead to the breakdown of the electrolyte and the dissolution of metal ions in the cathode, which can significantly accelerate LLI and LAM.

Over-charging/over-discharging generates much Joule heat, which can trigger the decomposition of electrolyte substances and lead to a cascade of side reactions, even cause the separator to rupture [54,55]. Under such circumstances, the electrode may dissolve or deteriorate, leading to short circuit [5,56]. When gas products are generated or significant volume expansion happens, the internal pressure is too high, directly bringing battery rupture, cracking, and chemical leakage, posing a safety hazard [57]. Mechanical stress is an essential parameter to reflect the battery performance under such complicated condition, cracking by external pressures (e.g., manufacturing pressure and the

 © Science China Press 2024

working load) and internal pressure (e.g., electrode material expansion and gas generated within the battery), showing a guideline to analyze potential cracking and dangerous accidents [58].

Other factors such as charge/discharge rate, operating conditions, and charge/discharge current can also significantly impact battery performance. The capacity of LIBs tends to decrease as the charge/discharge rate increases. Excessive charge/discharge rates can accelerate the degradation of electrolyte substances, raise the internal temperature of the battery, and hasten the lithium-ion plating process, leading to a shorter lifespan of the battery. Yuan *et al.* [58] explored the boundary conditions of charging/discharging rate of $LiFePO_4$ batteries and demonstrated experimentally that a maximum rate of 5 C (fully discharging within 0.2 h) can be achieved with the maximum voltage of 3.7 V.

In conclusion, various aging factors affect the battery performance and lifetime primarily by creating multiple internal degradation mechanisms. The LLI is primarily due to solid electrolyte generation and decomposition, metal electrode dissolution, lithium plating, and dendrite formation within the battery. Increases in IR are primarily caused by the generation and decomposition of SEI, electrode dissolution, and current collector corrosion. LAM manifests in various ways such as loss of electrical contact, electrode dissolution, and electrode particle cracking. These three primary degradation modes work in conjunction and are affected by several factors, resulting in nonlinear battery degradation that is challenging to predict.

TRADITIONAL TECHNOLOGIES FOR SOC, SOH AND RUL ESTIMATION

The evaluation of battery status involves the estimation of the performance degradation, range, and estimation of RUL using historical cycling as data source under various mathematical models. Accurate battery status estimation can provide end-users with a clear evaluation of the maximum remaining range, which can offer reliable advice for safe battery operation. Accurate battery status estimation can benefit battery producers by expediting the design of high-performance batteries that offer improved recycling utilization, lower operating costs, and increased safety and reliability. Under this context, the estimation of battery states has been an active area of research, with SOC, SOH, and RUL serving as the main indicators. We have summarized the prevailing estimation methods and discussed their strengths and limitations, with the goal of providing useful insights for future research on batteries.

SOC estimation

In definition, SOC is the ratio of the battery energy remaining currently to the fully charged energy, indicating how long the battery will last before a recharge is required [59]. The battery SOC is similar to the fuel gauge which is installed on a gasoline vehicle to determine the left fuel in the tank. However, directly measuring SOC can be challenging due to the nonlinear degradation of batteries. It is necessary to rely on other parameters (e.g., current, terminal voltage, and temperature) to estimate the battery SOC. Generally, SOC estimation methods can be classified into four categories: ampere-time integration, characterization parameters, model-based indicators, and data-driven analysis, as illustrated in Fig. 3.

Ampere-hour integral method

The ampere-hour (AH) integral method, also known as the coulomb counting method, is the major method used to calculate SOC. This method estimates SOC by utilizing the defining equation: ratio of the current remaining battery capacity to the

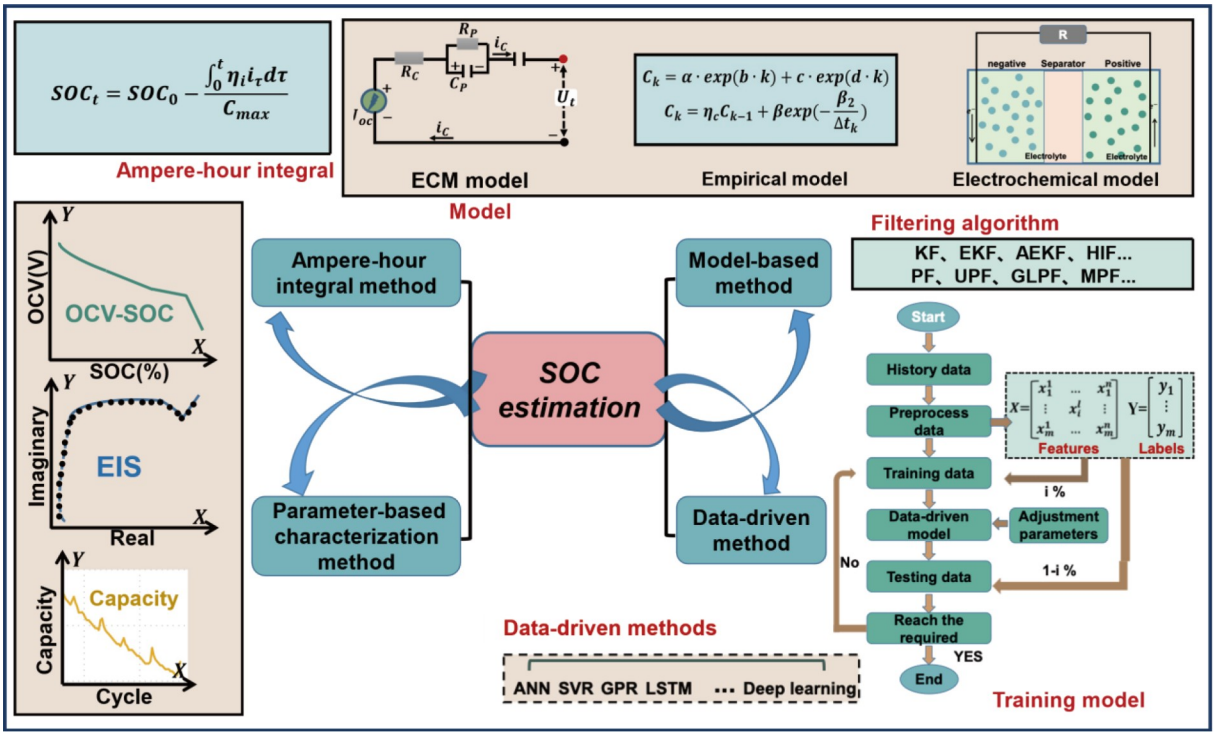

Figure 3 Methods of predicting the battery SOC.

© Science China Press 2024

maximum available capacity [60,61]:

$$\mathrm{SOC}(t) = \mathrm{SOC}(t_0) - \frac{\int_{t_0}^{t} \eta_i i_{(\tau)} \mathrm{d}\tau}{C_{\max}}, \quad (1)$$

where SOC(t) is the predicted SOC at moment t, SOC(t_0) is the initial value, η_i is the coulomb efficiency for charging/discharging, $i_{(\tau)}$ is the current at moment τ, and $C_{\max}$ is currently available maximum capacity.

The AH integral method provides excellent accuracy if the initial SOC is sufficiently accurate [62]. While its limitation is also obvious that the evaluation relies on the use of the static maximum capacity $C_{\max}$, which is strongly affected by battery performance degradation over time. Furthermore, obtaining an accurate initial value SOC(t_0) is particularly challenging, as these parameters are highly sensitive to external environmental factors, such as temperature and noise. Importantly, these uncertainties have a cumulative effect on the estimation error, impairing the estimation reliability. Therefore, the AH integral method is unsuitable for online applications.

Parameter-based characterization methods

Different from AH integration, the parameter-based characterization technique aims to identify the most stable and easily observable parameters, based on which a mapping relationship between SOC and observed quantity has been explored [63]. The key question is which parameters can be utilized to achieve this goal. So far, characterization parameters, including the current residual capacity [64], open-circuit voltage (OCV), electrochemical impedance spectroscopy (EIS), and IR (polarized IR and Ohmic resistance) [65,66], have been investigated. In practical applications, the OCV-SOC relationship, which is relatively stable, has been widely employed to calibrate the battery's SOC with reasonable accuracy. The SOC is related to the static thermodynamics inside the battery and the quantity of lithium ions intercalated in the active material, and each battery system thus has its own unique OCV curve. At the same temperature, the curve has a fixed relationship with the battery's SOC, which does not fluctuate considerably with the external environment or changes in operating conditions [18,67–70]. Severson *et al.* [71] took the capacity as a function of voltage and achieved an error of 4.9% in estimating battery capacity using only the first five cycles of voltage data. This success highlights the potential for accurately estimating the battery's SOC using the OCV, which can significantly improve predictability and accuracy in battery performance. For this method, the primary challenge lies in the OCV measurement, which exhibits hysteresis and requires a sufficient rest time to accurately assess the SOC. Thus it is not commonly utilized in studies examining the electrochemical performance of batteries [72,73]. EIS is a commonly used technique for investigating the internal chemistry of batteries. It assesses the SOC by detecting changes in resistance and capacitance at different frequencies of alternating current (AC) signals [74–76].

Although parameter-based characterization methods are widely used, the constant-current discharge mode used to determine the parameters in experiments is not practical for real-world applications. Additionally, an accurate mapping relationship between the SOC and characterization parameters must be obtained using checking tables and other methods, which lacks real-time feasibility and cannot effectively discriminate battery performance during operation.

Model-based approach

To avoid large lab-based measurement requested by parameter-based methods, a model-based approach has been proposed, focusing on the exploration of appropriate state estimation algorithms [77]. In the literature, three battery models have been proposed: the electrochemical model (EM), the equivalent-circuit model (ECM), and the black-box model (i.e., an empirical model) [78]. Based on these models, a series of mathematical equations, including partial differential or algebraic equations, have been utilized to predict the SOC. For instance, the EM describes the diffusion and migration of lithium ions, electrochemical reactions, charge conservation, Ohm's law, and other properties of the battery. Such model has been applied to depict the microscopic physicochemical reactions that occur within the battery based on clear physical meaning. Among various models, the pseudo-two-dimensional (P2D) model based on porous electrodes and concentrated solution theory, developed by Doyle *et al.* [79] in the 1990s, is the most widely used one. The P2D model utilizes the solid phase, liquid phase, and three regions (i.e., the positive electrode, negative electrode, and diaphragm) to describe battery characteristics, and it is based on several assumptions: (i) the solid phase is comprised of equal-sized spherical particles; (ii) the density and potential of the solution only move along the horizontal axis (i.e., diffusion and migration only occur in the X-direction); (iii) the electrochemical properties of the positive electrode, negative electrode, and solid–liquid phase interfaces can be well analyzed using a range of mathematical equations.

While the P2D model excels in simulating battery structures, it poses challenges due to the presence of numerous differential equations, demanding extensive computational resources and presenting a high level of complexity. Here, the ECM, which does not delve into the microscopic reaction mechanisms of batteries, boasts a relatively straightforward structure and stands out as another widely employed model-based approach. ECM utilizes the electrical behavior generated by circuit components to simulate external features such as the IR, voltage, and capacity of the battery. The ECM is highly versatile and applicable to various operating conditions, with significantly fewer state equations than other models. This makes it easier to analyze and solve, and it has been widely utilized in the modeling of EVs. Common ECMs include the Rint model, Thevenin model, Partnership for a New Generation of Vehicles model (PNGV), dual-polarization model, second-order RC model, and third-order RC model, among others, as illustrated in Fig. 4.

The Rint model is widely used for its simplicity and effectiveness. It includes an ideal voltage source and a constant IR. The terminal voltage and resistance of the model are obtained by measuring the OCV and load when the battery is fully charged. However, the Rint model exhibits an obvious voltage response to changes in load, and it does not account for variations in IR. As a result, it is limited in real application scenarios. To address this issue, Thevenin model has been proposed with better consideration of the dynamic behavior. It predicts the instantaneous voltage response to current load changes by adding more RC networks. However, the Thevenin model assumes that all electrical units are constant, which is incompatible with the real-world scenario throughout the battery cycle. Thus, it cannot simulate the battery running time or capacity decline associated

© Science China Press 2024

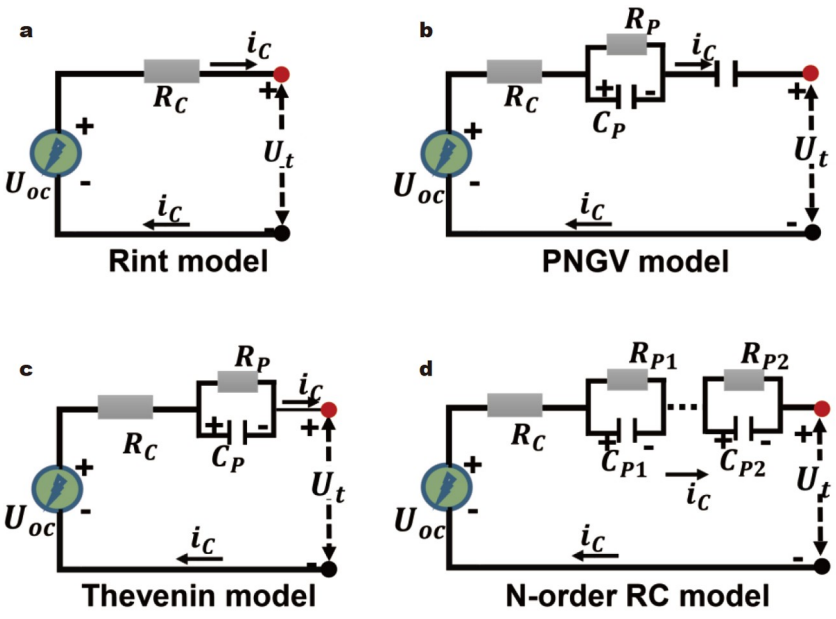

Figure 4 ECM models: (a) Rint model, (b) PNGV model, (c) Thevenin model, and (d) N-order RC model.

with thermal and degradation effects [11,80,81]. Moreover, more advanced models have been developed to achieve better performance, such as combining electric models that account for battery degradation and thermal effects, and run-time electrical models based on runtime. Hu *et al.* [82] experimentally confirmed that a first-order RC model with one-state hysteresis has higher estimation accuracy for $LiFePO_4$ batteries by fitting parameters to different ECMs. Additionally, a fractional order model has been established through the research on AC impedance and the ECM [83]. Yang *et al.* [84] proposed a simplified fractional-order impedance model and utilized a genetic algorithm to identify its parameters, achieving a maximum battery voltage tracking error of only 0.5%.

The black-box model, also known as the empirical model, collects common characteristics extracted from historical data and utilizes various regression models to fit these data. Such parameterized model is often used to study complex systems with many uncertain relationships, such as the battery's nonlinear degradation. The process of parameterization is typically complicated and heavily relies on the quality of training samples and the machine learning algorithm utilized. Furthermore, the empirical model solely focuses on the input and output data. It lacks interpretability regarding electrochemical mechanisms.

Model-based methods for SOC estimation begin with an initial SOC value and can generate two sets of OCV profiles: an experimental value obtained through the AH integral method and an actual value determined through model measurement. The calculated values are then continuously adjusted by gain calibration to minimize the error between the two OCV values. This process is repeated until the desired SOC estimation value is achieved clearly; the overall performance relies on the basic model and the following gain correction. So far, gain correction is commonly performed based on state estimation algorithms, such as Gaussian process (GP)-based filter and probability-based filter. For the former, several filter schemes have been proposed, including Kalman filter (KF) [85,86], unscented KF (UKF) [87], extended KF (EKF) [88–90], linear KF, adaptive extended KF (AEKF) [91], and H_∞ filter. Among which KF algorithm has been widely applied to linear battery models for SOH estimation. It is a two-step recursive process that involves forecasting the system state and output, while also constantly changing the state of the system in response to the output error [92–94]. Shrivastava *et al.* [95] combined a battery model with KF algorithm to predict SOC, and furthermore, considering nonlinear characteristics, advanced filtering methods such as EKF, AEKF, UKF, and square-root traceless KF methods were employed to address the effect of battery noise on SOC estimation, leading to significant improvements in the accuracy and robustness of the state estimation. The EKF is a suboptimal filter that linearizes the nonlinear system before KF. It uses partial derivatives to expand the nonlinearity function, but its linearization procedure frequently introduces truncation errors that can impair the accuracy of SOC estimation [96].

Different from KF filters, probability-based filters, such as particle filter (PF) [97,98], unscented PF (UPF), and cubature PF (CPF), are proposed based on the empirical distribution of the system space state vector. The PF fitting technique generates a set of discrete sampling points in the state space and adjusts their position and particle state based on observed values, and the optimal particle state can be obtained by continually modifying the particle set. Wang *et al.* [99] and Liu *et al.* [100] demonstrated that the PF method outperforms EKF and UKF in terms of the accuracy of SOC estimation. The UPF method improves the particle sampling process of PF by utilizing a posterior density function to compute the mean and variance of particles. This approach provides more estimation information and further enhances the accuracy of SOC estimation [101,102].

SOH estimation

SOH is an important metric for batteries that are in use and have begun to degrade. It provides a quantitative assessment of the changes in a battery's charge/discharge capacity and storage capacity over time. Essentially, SOH drops as batteries age and experience performance loss, and it cannot be accurately

 © Science China Press 2024

determined prior to the battery entering service. Therefore, monitoring SOH is crucial for predicting battery life and identifying when it may be time to replace a battery. Performance parameters that undergo significant changes with cycling and aging, such as the number of cycles, IR and capacity, can be used as crucial indicators for calculating SOH, and the classification criteria for estimating SOH vary across different literature [24,103,104]. This section provides an overview of the most common methods for estimating SOH, which include experimental analysis and model-based approaches [105,106]. Experimental analysis methods involve collecting data on a battery's voltage, current, and temperature under controlled laboratory conditions to analyze its aging behavior. This approach is commonly used to investigate the underlying aging mechanism and provide theoretical support for predicting battery SOH. Specifically, the experimental analysis method can be further classified into direct measurements and indirect analysis, as summarized in Fig. 5. Their advantages and limitations are also discussed in Table 1.

Direct measurement

The direct measurement methods for SOH can be categorized based on various characteristic parameters, including capacity/energy profiles, AH counting, Ohmic resistance tests, impedance-EIS spectra, cycle number counting, and destructive methods. Of these parameters, the capacity/energy test is the most fundamental and direct approach for evaluating SOH. Specifically, the capacity of a battery reflects the energy it can store when fully charged, and if the capacity is determined, the SOH of the battery can be ascertained [39,105]. Currently, battery capacity can be accurately and directly measured in a laboratory setting using online capacity identification devices such as BMS. However, the accuracy of capacity estimation depends heavily on the stability of the charge/discharge environment and cycle integrity, which can make real-time online measurements of operating batteries challenging. Apart from direct energy measurement, SOH can be evaluated using the AH counting method by

$$\mathrm{SOH} = \frac{Q_{\max}}{Q_{\mathrm{n}}} \times 100\%, \tag{2}$$

where Q_{n} and $Q_{\max}$ are the nominal capacity and the maximum available capacity in its current state. The precision of the AH counting method depends on the accuracy of the residual capacity measurement, which is inextricably linked to the use of high-precision current sensors. Ng *et al.* [107] utilized an enhanced Coulomb counting method to estimate the battery SOC and SOH under fully charged/discharged conditions. They achieved estimation error of 1%, which demonstrated the convenience and validity of this method in simulation experiments. However, meeting the instrumentation requirements of the AH counting method can be challenging in practical applications, and monitoring battery current over extended periods can be costly. Furthermore, the fully charged/discharged state occurs

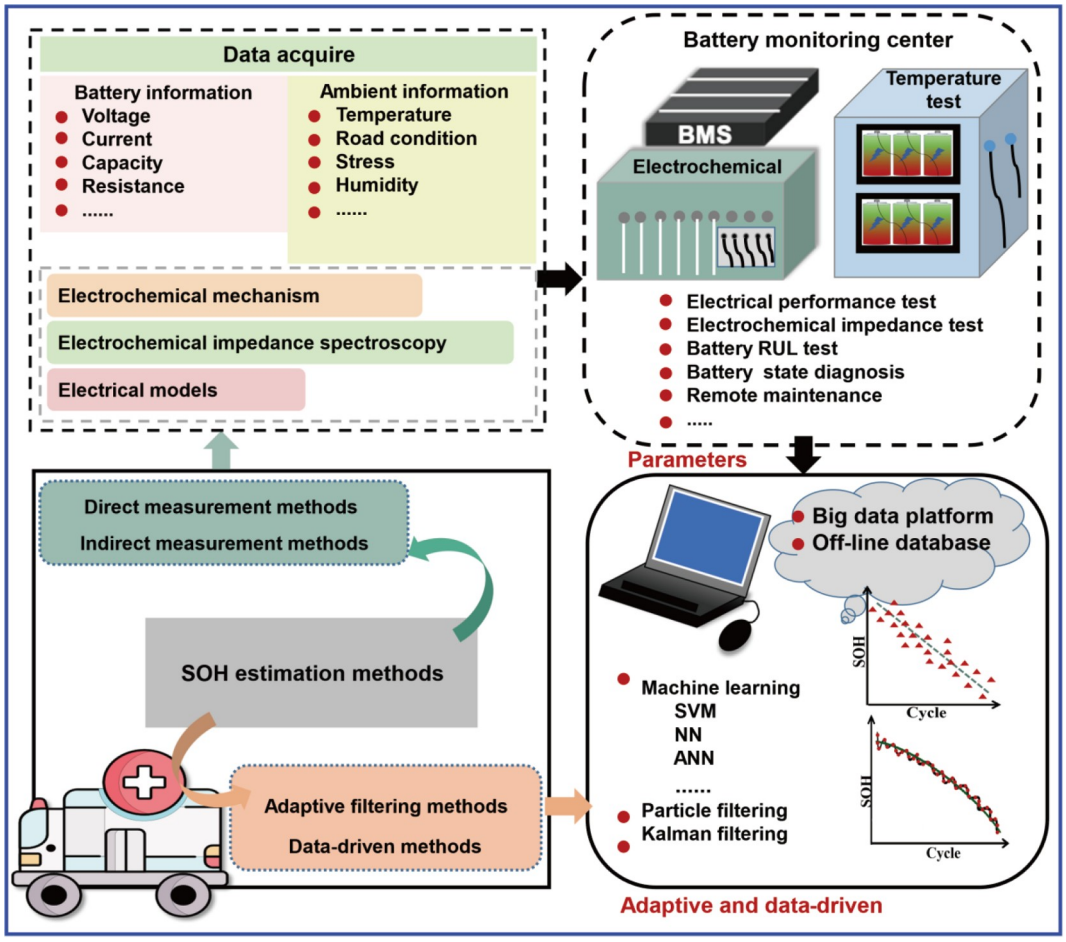

Figure 5 Brief introduction and classification of SOH estimation methods.

© Science China Press 2024

Table 1 Summary of SOH estimation methods

Category	Methods	Advantages	Disadvantages
Direct measure	Capacity/energy	Simple and easy to implement	Limited accuracy; susceptible to the environments and equipment
	AH counting	High precision	Depending on device accuracy; hard to operate online
	Ohmic resistance impedance	Good real-time performance; easy to implement and study the aging mechanism	Susceptible to the environments and equipment
	Cycle number counting	Easy operating; simplest and most straightforward	Not suitable for practical application
	Destructive approaches	Good for theory tests; easy to study the aging mechanism	Not suitable for practical application; may destroy the battery
Indirect analysis	IC/DV analysis	Interpretable; high accuracy	Difficult to operate in real time
	DTV/DMP	Applicable to theoretical study	Difficult to operate in real time
Adaptive algorithm	Joint estimation	High accuracy and robustness; easy operating online; combinable with other methods	Strongly depending on the accuracy of the models
Data-driven	Sample entropy, optimization algorithm, etc.	High accuracy; no complex model required	A large amount of calculations; poor interpretability; hard to adjust parameters

infrequently during EVs operation. As a result, this method is often used in laboratory settings to measure the change in residual capacity under a slight constant current charge/discharge and to verify the accuracy of other measurement methods [105].

The Ohmic resistance measurement method is used to directly estimate and evaluate battery SOH by measuring its IR [108,109]. In practice, IR has been split as Ohmic resistance and polarized IR. The former is simple and primarily determined by battery components, but its measurement accuracy is heavily affected by voltage and current fluctuations. The calculation formula is

$$R = \frac{\Delta_U}{\Delta_i}, \tag{3}$$

where R represents R_p or R_c, Δ_U is the pulse voltage variation of the battery and Δ_i is the pulse current variation. For practical operations, measurement can also be affected by the temperature, battery aging, and sampling interval. Therefore, a smaller interval for voltage and current sampling is often necessary to obtain a more accurate record of Ohmic resistance. Waag *et al.* [110] extensively investigated the nonlinearity of battery resistance, demonstrating that it varies slightly with SOC and varies with the temperature and battery life.

EIS is a widely researched method for determining the SOH of batteries. It measures the impedance of a battery at different frequencies, which exhibits primarily Ohmic characteristics at higher frequencies and capacitive traits at lower frequencies [104]. Electrochemical workstations and other AC excitation devices with similar functions are used to measure battery impedance at different frequencies. The obtained impedance spectra are then compared with EIS to determine the status of the battery [111–113]. Galeotti *et al.* [115] established a relationship between the Ohmic resistance and available capacity to calculate the SOH of the battery, showing a maximum evaluation error of 3.73%. Xia and Abu Qahouq [37] conducted research on predicting SOH by analyzing the relationship between AC impedance and capacity decline, demonstrating the relationship between the zero-crossing frequency and aging state. Following this result, the SOH was further assessed by incorporating the zero-crossing frequency as an input parameter in the neural network (NN) algorithm. Moreover, by incorporating auxiliary tools and carefully configuring the equipment parameters, any effects on the Ohmic resistance of EV devices during constant current charging/discharging can be minimized [116,117]. However, EIS has certain limitations that must be considered. For instance, significant performance fluctuations and poor generality between different battery types have been observed. In addition, EIS testing can be time-consuming and requires a stable testing environment, which may not always be available in practical applications.

Counting battery cycle number is the simplest and most direct way to evaluate the battery state. By using a BMS or other devices with counting capabilities to visualize the battery's cycle number, the health status of the battery can be measured by comparing the measured value with the total cycle number calibrated by the manufacturer. It is important to note that the cycle number is measured based on the assumption that the battery is deeply and completely discharged. For an incompletely discharged battery, it is necessary to measure the conversion coefficients under experimental conditions first and then convert them to fully charged/discharged cycles before calculating the SOH [105]. The destructive method is an additional approach to measuring the conventional electrical properties of batteries. It is a conventional approach used to predict the SOH of the battery, which can provide precise information about the battery's internal degradation [118]. The limitation is that such operation may harm the performance, resulting in irreversible damage. The commonly used destructive methods include atomic force microscopy (AFM), Raman spectroscopy (RS) [119], auger electron spectroscopy (AES), scanning electron microscopy (SEM), X-ray diffraction analysis (XRD) [40], and

© Science China Press 2024

cyclic voltammetry [106,120].

Indirect analysis method

In contrast to direct measurement, parameters can be indirectly obtained to determine SOH. Specifically, health indictors (HIs) that can reflect the change in batter capacity or IR, instead of directly measuring these parameters, are also effective approaches to calibrate the SOH. The HIs that are frequently mentioned include incremental capacity (IC), differential voltage (DV), voltage response trajectory, SEI membrane impedance variation, and constant-voltage charge/discharge time [75]. IC/DV analysis is a widely used technique in indirect analysis, employing IC and DV curves to examine battery degradation and aging mechanisms. It is well known that IC curve represents the relationship between the derivative of the capacity with respect to the terminal voltage and voltage change $\left(\frac{\mathrm{d}Q}{\mathrm{d}V} \rightarrow V\right)$. Conversely, the DV curve as the reciprocal of the IC curve, giving the relationship between the derivative of the voltage with respect to capacity and the capacity variation $(\frac{\mathrm{d}V}{\mathrm{d}Q} \rightarrow Q)$ [32]. IC and DV curves have distinct characteristic peaks, each with unique features, locations, and shapes that are determined by the electrochemical reactions occurring inside the battery [12,121]. For instance, the peaks observed in IC and DV curves correspond to electrochemical phase equilibrium and phase transition, respectively. By analyzing the shapes and positions of these characteristic peaks, microscopic chemical reactions and aging mechanisms can be investigated. Subsequently, a relationship between capacity and these characteristic values can be constructed [122]. It is worth mentioning that the position and height of the characteristic peaks in IC/DV curves may vary depending on the battery's status and the starting time of the charge cycle [30]. Unlike the DV curve that represents the relationship with capacity, which decreases continuously with battery aging, the IC curve indicates the relationship with voltage, is less susceptible to polarization, and has a more stable peak position, resulting in direct and reliable measurement results. Weng *et al.* [123] calculated the battery SOH based on IC curves and experimentally demonstrated that its peak height decreases as the battery capacity reduced. In the laboratory, charge/discharge experiments with lower multipliers (e.g., C/20, C/3) are performed to measure peak variation, because a higher multiplier generates large impedance that offsets the peak variation and leads to errors. IC/DV analysis requires only the measurement of battery capacity and voltage changes, which can be done easily and conveniently using well-established BMS. However, the differential process makes the curve highly sensitive to external factors such as temperature, noise, and battery performance, and thus data noise must be reduced or eliminated before analysis using various filtering algorithms, such as Gaussian filtering and particle filtering [124].

Differential thermal voltammetry (DTV) analysis and differential mechanical parameter (DMP) analysis are two other commonly used methods for calculating the SOH of batteries, which are often utilized as complementary tools to IC/DV analysis. DTV analysis combines IC measurement and temperature monitoring to obtain thermodynamic information such as the temperature variation with time ($\mathrm{d}T/\mathrm{d}t$) and entropy. Recorded spectrograms are then used to detect the changes in characteristics such as the peak position and amplitude, providing an indirect reflection of battery status. Maher and Yazami [40] validated that the peak and height of entropy variation in the spectrum are comparable to the IC/DV, confirming that the SOH can be measured through DTV. Merla *et al.* [125] conducted an investigation on the DTV spectrum and discovered that the height and location of the spectral peak are related to the impedance, which varies with the battery ages. It is noted that the entropy/enthalpy change curves do not align completely with the battery discharge and open circuit potential (OCP) curves. Using thermodynamic techniques, Maher and Yazami [40] calculated the capacity loss and discharging potential of batteries under constant-current charging and C/2 discharge cycles. Their experiments showed that with an increase in the number of cycles, the changes in the entropy and enthalpy curves were more significant compared with the discharge or OCP curve.

The DMP method focuses on mechanical properties, as the volume change of the battery is believed to be connected to the development of an SEI film throughout the battery cycle. Load sensors have been utilized to measure mechanical stress (stress-strain) variations in the battery, and experimental results have demonstrated that the stress produced during battery charging/discharging is positively correlated with the battery SOH [44]. In an experiment, the SOH can be measured by utilizing the relationships between strain/stress and capacity/voltage. However, the DMP approach is only suitable for battery systems that can expand freely and is challenging to apply to battery packs with limited space. After measuring the stress at the end plates of a battery pack, Samad *et al.* [64] developed a force-based IC curve to estimate the battery capacity $\left(\frac{\mathrm{d}Q}{\mathrm{d}F}\right)$. They found that the capacity decay is linearly correlated to the peak voltage. The proposed ICF method showed a capacity estimation accuracy of 0.42% during low-C-rate constant-current discharge.

Adaptive algorithm

The adaptive algorithm continuously updates the model parameters based on a battery model to accurately estimate the SOH, and the specific models, such as EM and ECM, have been described in the previous section [126]. The adaptive algorithm is characterized by the simultaneous implementation of model parameters, online updating, and SOC estimation. It can be divided into three types: joint estimation, collaborative estimation, and fusion method. After obtaining the SOC, the SOH is calibrated accordingly, and the model parameters are continuously optimized using feedback from new measurements until the desired level of predicted error is achieved. There are various approaches for updating the parameters in adaptive algorithms, such as the KF, PF [127], and least-squares algorithms. These methods contribute to the continuous improvement and refinement of the model's accuracy.

The joint estimation method commonly employs multiple filters to measure the model parameters and estimate the battery's SOC. The model parameters consist of the IR, current, voltage, capacity, OCV, and other related parameters mentioned earlier. Yu *et al.* [128] employed a joint estimation method that utilized two filters, namely the H-infinity filter and UKF, to estimate the battery's SOC online. The experiments revealed that the joint estimation method has superior accuracy, robustness, and adaptability in estimating the battery SOC compared with

 © Science China Press 2024

measurements taken for fixed parameters under different temperatures and loading. Wei *et al.* [129] introduced a dual-estimation method that integrates the KF-based SOC estimator and a novel recursive least squares (RLS)-based capacity estimator. Their experimental results indicate that the proposed model parameters, SOC, and capacity can be computed in real-time with rapid convergence and high accuracy. Moreover, in practical applications, the joint estimation method outperforms other existing approaches in terms of computational cost.

The collaborative estimation method shares similarities with the joint-estimation method, as both involve simultaneous online prognosis of model parameters and SOC. However, the former also includes an assessment of battery capacity. The primary difference between these two approaches lies in the fundamental frameworks of the algorithms utilized. This manifests in two ways: (1) the relationship between the parameter and state estimation and (2) the model used to obtain the terminal voltage error (i.e., the new information for updating). In the joint estimation method, the voltage errors in the two estimators are independent, which implies that there is no significant interaction or correlation between the predicted results for the parameter and state. In contrast, the collaborative estimation method utilizes a single voltage error for both estimators, indicating an apparent interaction between the state and parameter prognosis.

RUL prediction

The RUL is a crucial battery parameter that is determined by comparing the performance and state of an old battery with that of a new battery of the same type [11,130]. The RUL is determined by calculating the remaining time and number of cycles until the battery's performance falls below the failure threshold, which requires full consideration of the battery status, historical cycle data, failure mechanisms, capacity decline trajectory, and other battery properties [75]. For instance, RUL defined in terms of cycles can be expressed as

$$\mathrm{RUL} = m - n, \tag{4}$$

where m is the overall cycles at the battery's end of life (EOL), and n is the current cycle number [24]. So far, research on RUL prediction for batteries has employed two main approaches: mechanism analysis and data-driven methods [131]. The former is based on the physical principles and concepts underlying battery chemical reactions, which require precise modeling and parameter settings. However, it is not well-suited for real-time operations due to the extensive number of intricate mathematical computations that it involves. Currently, data-driven methods are the most promising approach for estimating battery RUL, as illustrated in Fig. 6, which can be categorized into three types: empirical, filtering, and time-series methods. The empirical method is founded on the concept of data fitting, where the RUL prediction is accomplished by fitting a mathematical model to aging data that describe the aging behavior of the battery. However, identifying an appropriate mathematical model requires multiple attempts to ensure the model is well-fitted, accurate, and robust. Commonly used empirical models include polynomial, single-exponential, double-exponential, Verhulst, and others. Additionally, methods for predicting RUL can also be classified into AI, filtering, and stochastic processes [132]. This section provides a detailed explanation of various approaches used for forecasting the battery RUL.

AI/time-series prediction

This approach views battery RUL as a time-based problem, analyzing historical data generation patterns in time series and using diverse models to forecast battery degradation trends. Time-series modeling can be categorized into two types: traditional modeling, which focuses on univariate time prediction, and machine learning methods, which tackle multivariate time prediction. Traditional univariate forecasting models include moving average (MA), autoregressive moving average (ARMA), and autoregressive (AR) models. In contrast, the support vector machine (SVM), relevance vector machine (RVM), and random

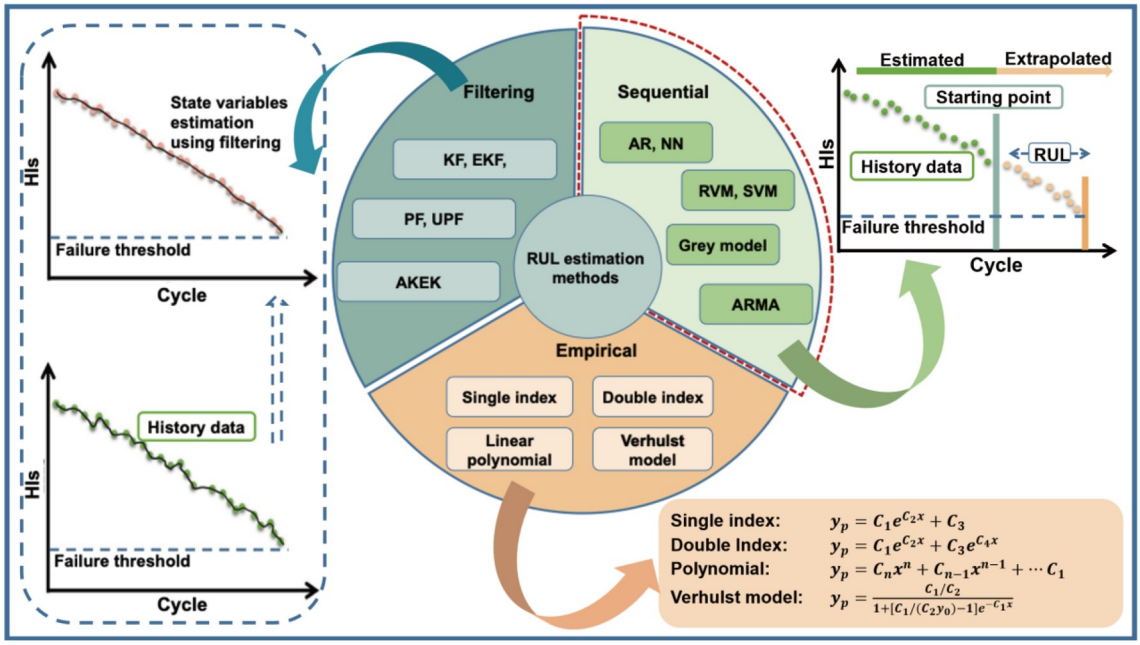

Figure 6 Data-driven approaches for estimating the RUL.

© Science China Press 2024

forest (RF) methods, etc., are common time-series forecasting methods based on machine learning models [133]. Without requiring a physical model, battery RUL can be estimated by fitting a variable model from monitoring data and then extrapolating the variables to a failure threshold, as outlined in Fig. 7.

Filter prediction method

Filtering methodology is mainly derived from Bayesian filtering and Monte Carlo simulation, both of which are based on the concept of state estimation [134]. Monte Carlo simulation calculates the posterior probability density by generating a large set of random particles and accumulating their correlation weights. The filtering algorithm uses real-time data to continuously update the battery parameters and then improves fitting quality using the empirical prediction method. The algorithm is not limited to a single state space, which provides reasonable probability estimates for Gaussian, non-Gaussian, and nonlinear systems. Commonly used filtering techniques include KF, EKF [135], PF [136], and UPF, as introduced in section of "SOC estimation". It has been shown that full consideration of operating conditions is efficient to predict the battery RUL by combining various filtering methods with existing diagnostic techniques, such as Bayesian, naive Bayesian, and sparse Bayesian techniques, [137,138]. Xing *et al.* [97] adopted an integrated model and utilized the PF algorithm to adjust model parameters and predict the remaining capacity of batteries. Their study demonstrated that the proposed method outperformed both exponential and polynomial models, showing better regression characteristics, robustness, and effectiveness, as well as smaller errors and standard deviations. Additionally, Yang *et al.* [139] proposed a model-based Bayesian approach for predicting the RUL. They utilized a logarithmic model to capture the trend of $Li(NiMnCo)O_2$ battery degradation and demonstrated that the addition of filtering improves the accuracy of the predictions, surpassing that of existing double-exponential models.

Stochastic process

The stochastic process considers the temporal dependence of the battery cycling mechanism, which can be determined by giving the probability distribution of each finite subset for the variable $f(x_i)$ consistently. In contrast with AI, the stochastic process represents the uncertainty of prediction results but requires many complex mathematical calculations, and it generally includes a GP [140–142] and Wiener process (WP) [143]. The former is defined as the collection of a finite number of random variables: $\{f(x_i) \mid x_i \in x\}$ indexed by a set x, where x is the number of charge/discharge cycles and $f(x)$ is the mean or covariance function of x [144–146]. GP calculation has the advantages of flexibility, probability, and non-parameterization, and it incorporates prior knowledge of the data within a Bayesian framework to predict the system. Liu *et al.* [147] employed GP regression (GPR) and utilized the mean and variance to depict the level of uncertainty in assessing the SOH. The experimental findings suggest that the proposed approach has the ability to make precise estimation for LIBs. Furthermore, the performance of GP has been evaluated against other machine learning algorithms like SVM, RVM, and NN using simulation and experimental datasets. The results demonstrate that GP excels in quantifying the estimation uncertainty and evaluating nonlinear battery systems [144].

The WP is a continuous time stochastic process. Adopting the WP, Tang *et al.* [143] used a truncated normal distribution (TND) to model the battery state and obtained an accurate and closed battery RUL distribution considering measuring errors and drift parameters. Current research on WP is primarily centered around exploring the impact of WP and WP measurement errors on RUL prediction, offline parameter estimation (typically through maximum likelihood estimation), and

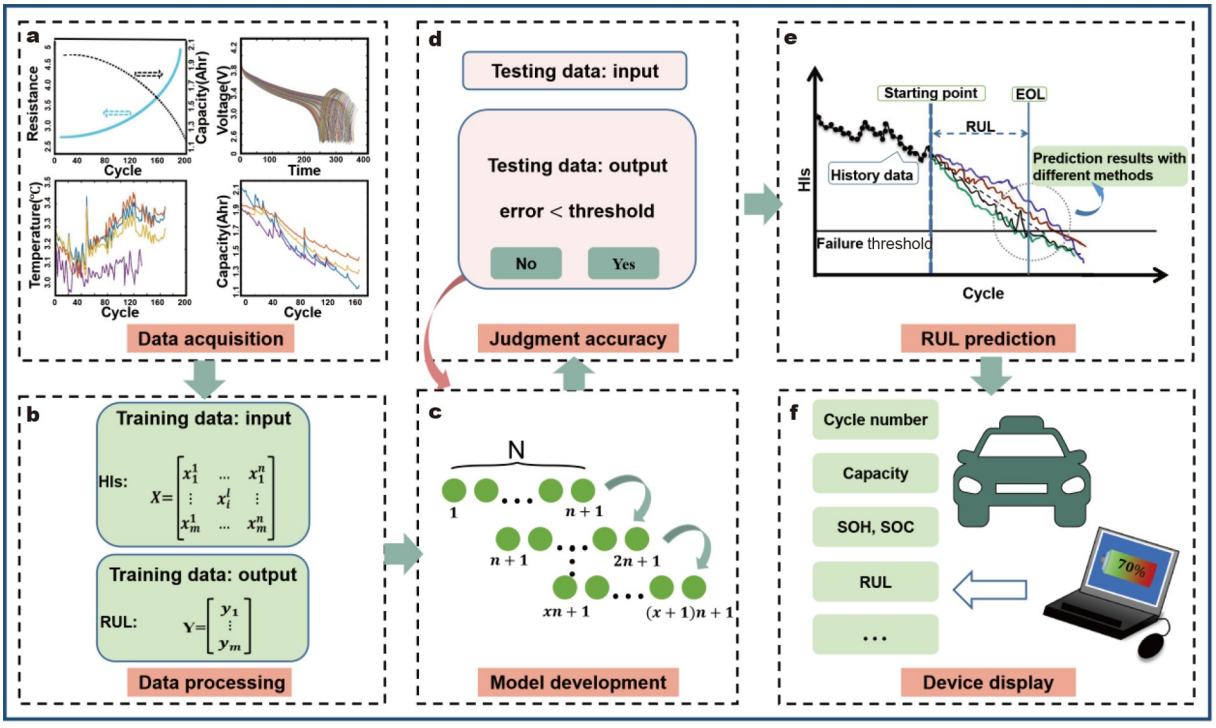

Figure 7 Specific steps in estimating the RUL with an AI approach.

© Science China Press 2024

updating the random parameters of WP metric error.

MACHINE LEARNING METHODS FOR SOC, SOH AND RUL ESTIMATION

Data-driven estimation

Data-driven methods utilize the large amount of offline data generated during battery cycles to establish and train a mapping relationship between the HIs and SOC, SOH, and RUL. By extracting information on battery aging from historical cycling data and using specific algorithms, HIs such as voltage, current, capacity, temperature, and IR can be extracted and the aging trend can be calculated [148–152]. One key advantage of data-driven methods is that they do not require complex models or reaction mechanisms. Instead, they only rely on the collection of battery aging data, which is particularly valuable for nonlinear correlation matters. However, data-driven methods rely on numerous offline data as prior knowledge for model training, which is essential for algorithm selection and can often be highly complex. Moreover, the aging data can be affected by battery system operating modes, cut-off conditions, and application requirements, which can result in varying generalization capability and poor robustness of trained models. Typical data-driven methods are NN, artificial NN (ANN) [37,153,154], SVM [155], RF and other machine learning and deep learning methods, among which, the empirical fitting methods are the simplest and easiest data-driven methods to implement, using basis set with polynomial, logarithmic, power, trigonometric, and exponential functions. Such fitting methods, however, often have poor accuracy and applicability due to the nonlinear nature of battery aging. To improve accuracy, optimization algorithms and sample entropy can be used to assess the predictability of time series and the regularity of data sequences. For instance, Widodo *et al.* [156] improved the accuracy of empirical fitting by incorporating sample entropy as an input for the learning algorithm. While this approach has been proven effective, it requires extensive calculations and data collection on battery aging, making it time-consuming and challenging to perform [44,156]. This section summarizes the general basic steps of various data-driven prediction algorithms, namely data acquisition, model training, and model testing [157]. The specific characteristics of each algorithm are given in detail in section of "Machine learning algorithms" [158].

Data acquisition

High-quality offline data are the foundation for model training, and performance evaluation for learning algorithm in terms of stability and reliability. Currently, a great deal of battery behavior can be collected during the cycling using existing test platforms and BMS, such as conventional electrical test, AC impedance, and remaining-life measurement. Other tests, like maximum available capacity, OCV, mixed pulse, EIS, discharge time, IR, temperature, and other original data also can be collected in a short time by controlling the operating parameters under well-defined experimental conditions. Severson *et al.* [71] generated a comprehensive dataset for 124 commercial lithium-ion phosphate/graphite batteries cycled under fast charging conditions. Impressively, their experiments provide comprehensive data about capacity degradation with a 3.6 C charge/discharge profile, the capacity decreased only 4% within 1000 cycles for most samples and some battery life even reached 2300 cycles. As battery aging tests are time-consuming and costly, and require complex and expensive signal acquisition systems, publicly available datasets are highly valuable for validating prediction algorithms [38], e.g., the National Aeronautics and Space Agency [159], Center for Advanced Life Cycle Engineering (CALCE) at the University of Maryland, University of Oxford, and Stanford University. Prior to model training, the raw data must be preprocessed with the primary goal of selecting relevant features, integrating and normalizing the data into appropriate blocks [149,157]. Algorithms can achieve high accuracy by selecting appropriate features that correlate with the state of the battery. The lack of key features can impair the model fitting and prediction quality, but having too many features can lead to model overfitting, making the model not universally applicable and lacking in prognosis ability. Data integration, normalization, and chunking are the process of organizing features in the required format, removing invalid data, and dividing the organized data into a training set, validation set, and test set for subsequent model processing [129,157].

Model training

To ensure accurate estimations, a well-trained model is essential, which can be achieved by using a validation set to assess linearity or nonlinearity and physical interpretability. The process of model training involves fine-tuning parameters to improve accuracy until further changes do not enhance the evaluation performance. Following this, the parametrized model is validated using a testing set to assess its robustness and precision.

Model testing

After effective training of the model, its capacity needs to be validated within an acceptable margin of error. If the validation falls outside this margin, further training or a new model is required until the ideal HIs and model are obtained. Compared with model-based methods, data-driven approaches do not consider chemical reactions. Instead, they rely on a mathematical module powered by weight parameters and embedded criteria, rather than a specific physics-based model. Thanks to the rapid development of computational efficiency, data-driven methods have a strong fitting ability under such a scheme, providing excellent self-adaptability to suit any battery and delivering versatile performance in real-world applications in recent years. Ni *et al.* [160] for instance, employed a data-driven approach to accurately predict the capacity decay curve of $LiFeO_4$ batteries. They successfully predicted the capacity loss using only the first 10% of the raw data, achieving an error of only 2.18%. With the rapid development of high-performance computational clusters, deep learning has been gradually applied to the prediction of battery nonlinear systems because it does not require manual design features.

Machine learning algorithms

Machine learning is realizing its promise with the advancement of computer science, especially in the case that a problem can be transformed into a classification, regression, or clustering task. Such tasks are critical aspects of machine learning and have been extensively researched [161–163]. Fortunately, the estimation of SOC, SOH, or RUL can be abstracted as a regression task, allowing us to deal with battery issues using powerful machine learning approaches, even without the background knowledge of

 © Science China Press 2024

the physicochemical materials and complicated reactions. To power such process, we simply need to conduct enough experiments to collect the battery parameters and corresponding experimental results, based on which a regression model has been constructed and trained with a large set of parameters, until the model correctly predicts battery features of interest.

Regression is an important supervised machine-learning problem, where the goal is to construct a model from many input data in predicting the continuous output. Classification differs from other supervised learning problems in that the input data are a feature vector of samples, but the output is the sample label and manifests as a one-hot vector. Formally, the regression task is to learn a function $f: X \to y$, where $X \in R^{n \times d}$ is the feature matrix, n is the number of samples, each feature vector has d dimensions, and $y \in R^n$ is the continuous target value vector. This is a common paradigm in real-world house price prediction, stock price prediction, and rainfall forecasting. In the following subsections, we summarize these newly developed techniques under the context of lithium batteries, focusing on the performance aging.

Linear regression (LR)

In machine learning, sample features and target properties (like battery performance) are described by a set of feature vectors X and target value y for each sample, using $\hat{y}$ denoting the predicted value. Before we describe the methods of LR, we first need to make several assumptions to guarantee that LR works well [164].

Each value of X and y is credible and from the real world.

The target value y can be linearly composed of feature vectors in X and model parameters w.

The variance of the errors is constant, and the values of the errors are serially independent.

The features in X are linearly independent of each other.

If all the above assumptions are satisfied, we can construct the LR model [165] as

$$\hat{y}(w, x) = w_0 + w_1 x_n + \ldots + w_n x_n, \tag{5}$$

where $w_1 \ldots w_n$ are weight parameters of the LR model and w_0 is the bias, which is called the intercept. Controlling the weights and bias in the 2D space uniquely determines a linear function. To find the line that best fits the data points, the LR model should optimize one loss function, i.e., minimize the residual sum of squares of the difference between actual and predicted values,

$$\min_w \|Xw - y\|_2^2. \tag{6}$$

This loss function can be solved easily using any well-established optimization method (e.g., the gradient descent method) or, if the feature matrix X is of full rank, we directly obtain the best parameter using the least-squares estimator $w = (X^T X)^{-1} X^T y$. This LR method is well known in the fields of statistics and finance for its simplicity and efficiency.

LR is now frequently combined with other methods or models to improve forecasting accuracy owing to its limited fitting performance; e.g., LR is combined with statistical analysis to accurately estimate battery OCV, which is critical in predicting SOH and SOC [166]. Furthermore, Hong *et al.* [167], by combining multiple LR and long short-term memory (LSTM) algorithms, proposed the LR-LSTM joint prediction model to achieve control of the prediction accuracy and horizon of the battery.

Ridge regression

Using the least-squares estimator to get the best parameters requires $X^T X$ to be reversible, which may be not satisfied, under which the data are referred to as having a multicollinear feature. Using a strong optimizer to minimize the loss function often leads to overfitting, meaning excellent performance on the training data but poor performance on the test data. In this case, a regularization technique is introduced. Ridge regression (RR) [168] sets an $l-2$ norm on the original LR loss function:

$$\min_w \|Xw - y\|_2^2 + \alpha \|w\|_2^2, \tag{7}$$

where α is a trade-off parameter of the loss function. The second term of the ridge regression loss function controls the sum of all parameters w. An increase in α decreases the sum of w and reduces unimportant parameters in w to almost zero, helping the model to learn a looser result and preventing the overfitting problem. From the perspective of the least-squares estimator, when adding an extra regularization item to the loss function, the closed-form solution of w changes as $(X^T X + \alpha I)^{-1} X^T y$, where I is the unit matrix. This formula is always reversible.

Least absolute shrinkage and selection operator (lasso) regression [169] is similar to ridge regression. In lasso regression, the $l-2$ norm is replaced with the $l-1$ norm:

$$\min_w \|Xw - y\|_2^2 + \alpha \|w\|_1^2. \tag{8}$$

Compared with the case of ridge regression, the $l-2$ norm indeed shrinks $\sum_{i=1}^{n} w_i^2$ to reduce overfitting, but the irrelevant parameters in w still exist. Thus, the covariate selection characteristics are weak, and the model is less interpretable. The $l-1$ norm is a stronger penalty than the $l-2$ norm, and it directly reduces the irrelevant parameter to zero rather than close to zero. This results in a model with only a few parameters that work in the end, and these features have non-zero values and are the key features of the model. Ridge and lasso regression methods counter the effects of multicollinearity, using a ridge to simulate the aging process of batteries. Wu *et al.* [170] obtained SOH estimation more reliable than those from nonlinear regression even though using less computing resources. Jiang *et al.* [171] compared the experimental performances of three regression methods in predicting battery SOH, finding that both ordinary least-squares regression and ridge regression had errors within 2% and that ridge regression had a smaller root-mean-square error.

Elastic-net regression combines the concepts of ridge and lasso regressions by introducing both $l-1$ and $l-2$ norms to the vanilla LR loss function:

$$\min_w \|Xw - y\|_2^2 + \alpha\rho \|w\|_1 + \frac{\alpha(1-\rho)}{2} \|w\|_2^2, \tag{9}$$

where α and ρ are trade-off parameters of the loss function. This joint formula retains the advantages of the two original methods while suppressing their disadvantages. For ridge regression, as we discussed before, it is difficult to select a covariate because the $l-2$ norm only shrinks the unrelated parameters down to close to zero. For lasso regression, the $l-1$ norm is sometimes too powerful. If a group of features are collinear, then lasso regression tends to select only one of the features, resulting in the excessive loss of information from the features. A reasonable

© Science China Press 2024

setting of the trade-off parameters in the elastic net thus leads to a suitable covariate selection result. Elastic-net regression has a wide range of applications. Lin *et al.* [172], for example, proposed a data-driven method for predicting the RUL, using elastic-net regression to extract characteristic features. Severson *et al.* [71] used machine learning to predict the RUL and classify the battery according to its cycle life. They generated model characteristics and used them in the elastic net, resulting in prediction error of 9.1% for the first 100 cycles.

Overall, three methods introduce regularization techniques to improve the prediction performance and perform well. To minimize the value of the loss function that we design for the model, the overfitting during the training process may occur and must be seriously considered. However, regularization approach can largely alleviate overfitting and ensure the model obtains a more relaxed result.

Support vector regression

SVM is a well-known robust machine learning method used for classification, regression, and outlier detection. Support vector regression (SVR) involves using an SVM model for regression [173], creating a spacing band on both sides of the linear object function $f(x) = wx + b$. The interval of this spacing band is denoted ε (often given empirically). We do not calculate the loss for all samples that fall into the spacing band, i.e., only the support vector affects the function. The optimized model is obtained by minimizing the total loss and interval. Here, we want the model parameters w to be as small as possible to keep the model robust. As for lasso regression, we add an $l-2$ norm to the function, and the problem is formally written as

$$\begin{aligned}&\min_w \frac{1}{2}\|w\|_2^2,\\ &\text{s.t.} y_i - wx_i - b \leqslant \varepsilon,\\ &wx_i + b - y_i \leqslant \varepsilon.\end{aligned} \tag{10}$$

Equation (10) is a hard-margin optimization problem. It is assumed that there is always a linear function $f(x)$ that satisfies the constraint. However, the real-world scenario is more complex, and we cannot find such an f. We therefore loosen the constraint with slack variables ξ_i and ξ_i' and obtain a soft margin loss function:

$$\begin{aligned}&\min_w \frac{1}{2}\|w\|_2^2 + C\sum_{i=1}^{n}\left(\xi_i + \xi_i'\right),\\ &\text{s.t.} y_i - f(x_i) \leqslant \epsilon + \xi_i,\\ &f(x_i) - y_i \leqslant \epsilon + \xi_i', \xi_i, \xi_i' \geqslant 0,\end{aligned} \tag{11}$$

where $C > 0$ is a box constraint that helps prevent overfitting. Equation (12) is a classical quadratic programming problem. Generally, we transfer the original problem to a more easily solved dual problem to optimize [174]. We first construct a Lagrange function of Equation (12) as the primal objective function:

$$\begin{aligned}&L = \frac{1}{2}\|w\|_2^2 + C\sum_{i=1}^{n}\left(\xi_i + \xi_i'\right) - \sum_{i=1}^{n}\left(\eta_i\xi_i + \eta_i'\xi_i'\right)\\ &-\sum_{i=1}^{n}\alpha_i\left(\epsilon + \xi_i - y_i + f(x_i)\right) - \sum_{i=1}^{n}\alpha_i'\left(\epsilon + \xi_i' - y_i + f(x_i)\right),\\ &\text{s.t.}\alpha_i, \alpha_i', \eta_i, \eta_i' \leqslant 0,\end{aligned} \tag{12}$$

where L is the Lagrangian and η_i, η_i', α_i, and α_i' are Lagrange multipliers. Continuing with the calculation of partial derivatives for the model parameters, substituting into Equation (12) and considering the Karush–Kuhn–Tucker conditions, we obtain a dual-objective function:

$$\begin{aligned}&\max_{\alpha_i, \alpha_i'}\frac{1}{2}\sum_{i,j=1}^{n}(\alpha_i - \alpha_i')\left(\alpha_j - \alpha_j'\right)x_i^T x_j\\ &-\epsilon\sum_{i=1}^{n}(\alpha_i + \alpha_i') + \sum_{i=1}^{n}y_i(\alpha_i - \alpha_i'),\\ &\text{s.t.}\sum_{i=1}^{n}(\alpha_i - \alpha_i') = 0,\\ &\alpha_i, \alpha_i' \in [0, C],\\ &\text{with KKT conditions } \alpha_i\left(f(x_i) - y_i + \epsilon + \xi_i\right) = 0,\\ &\alpha_i\left(y_i - f(x_i) + \epsilon + \xi_i'\right) = 0,\\ &(C - \alpha)\xi_i = 0,\\ &(C - \alpha)\xi_i' = 0.\end{aligned} \tag{13}$$

Sequential minimal optimization is the most popular method of solving a dual-objective function [175]. Once optimal α_i and α_i' are obtained, $f(x)$ can be written as

$$f(x) = \sum_{i=1}^{n}(\alpha_i - \alpha_i')x_i^T x + b, \tag{14}$$

where b is calculated using each support vector:

$$b = \frac{1}{|S|}\sum_{i\in S}\left(y_i + \epsilon - \sum_{j\in S}\left(\alpha_j - \alpha_j'\right)x_j^T x_i\right). \tag{15}$$

For a training sample x_i, if the corresponding $\alpha_i - \alpha_i' \neq 0$, we have a support vector, which means that x_i is located outside the spacing band. The support vector of SVR is only a small fraction of the training sample; thus, its solution is sparse and robust. SVR is illustrated in Fig. 8a.

One important limitation of the above regression methods is that they assume the relationship between X and y to be linear; however, most real-world data are nonlinear. To solve the nonlinear regression problem, Cortes and Vapnik [176] proposed the kernel method. The idea is that if a data set is nonlinear in a lower-dimensional space, we can map it to a higher- or infinite-dimensional space. The distribution of data points is sparser in higher-dimensional space, and it is thus guaranteed that there is a hyperplane containing all sample points, resulting in a linear data set and efficient and low-bias models. Li *et al.* [177] adopted a particle swarm optimization algorithm to optimize the parameters of the SVM model when predicting the battery SOC and performed cross-validation to evaluate the model's performance, confirming that the proposed model has higher accuracy and robustness.

The key point of the kernel method is to find a suitable kernel function. Formally, using Mercer's theorem [178], the kernel function is defined as follows:

Definition 1. Assume $\mathcal{X}$ is the input space and $\mathcal{H}$ is the Hilbert feature space. If there exists a mapping function $\phi(x): \mathcal{X} \to \mathcal{H}$, for all $x, z \in \mathcal{X}$, function $K(x, z)$ satisfies $K(x, z) = \langle\phi(x), \phi(z)\rangle$. Function K is then called a kernel function. Here $\phi(x)$ is the map

 © Science China Press 2024

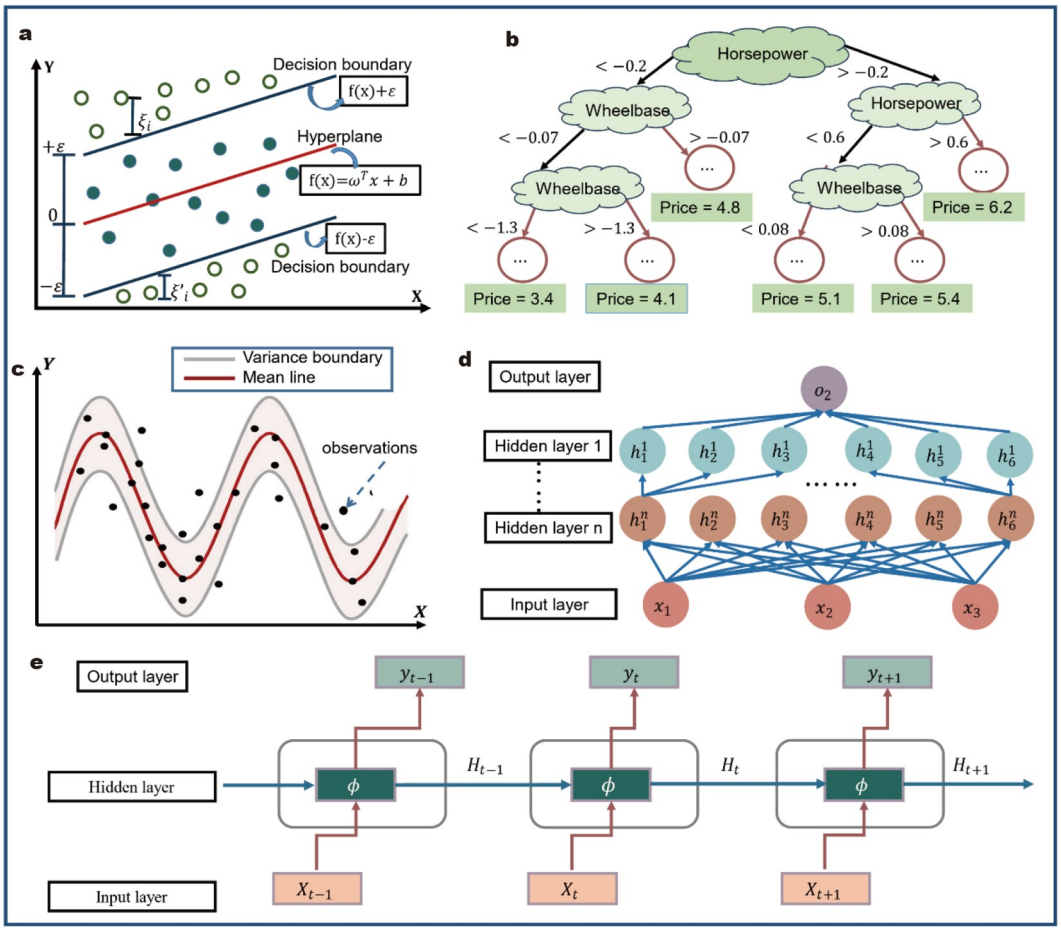

Figure 8 Illustrations of the data-driven approaches. (a) Diagram of the SVR structure. The loss for all samples that fall into the spacing band is zero. (b) Example of a regression tree structure for predicting the price of a car. (c) Illustration of the GPR structure. There are an infinite number of curves in the data. Each follows a probability distribution, and we find the curve with the highest probability. The figure plots such a curve with its corresponding probability distribution, described by the mean and variance. (d) FNN illustration. It is a multilayer perceptron, i.e., there are several hidden layers, and the nodes are fully connected. (e) RNN illustration. Each node value is affected by both the previous and subsequent moments.

function and $\langle\cdot,\cdot\rangle$ is the inner product space, mapping the input space to the high-dimensional space, but this map function is usually difficult to design. Even if we find a suitable mapping function, the computational overhead of calculating the inner product is vast if the dimensionality of the input features is high. Luckily, most regression or classification machine learning methods only need the calculation of the inner product of the input vectors, just like in SVR (Equations (13) and (14)).

$$f(x)=\sum_{i=1}^{n}(\alpha_i-\alpha_i')K(x_i,x)+b. \tag{16}$$

The kernel function helps us omitting the map function $\phi(x)$ and directly obtain the inner product, i.e., we can explicitly construct a kernel function $K(\cdot,\cdot)$ for a given $\phi(x)$ or we can take a kernel function and use it without having an explicit representation of $\phi(x)$.

GPR

Another application of kernel function in regression problems is GPR. This method considers the estimation of the regression problem from a probabilistic standpoint, which provides a rigorous model derivation and a strong guarantee of classical stochastic process theory. The method has natural advantages in terms of algorithm interpretability, model transparency, and uncertainty portrayal.

We start with a basic linear formula:

$$y=x^TW+\epsilon,\epsilon\sim N(0,\sigma^2), \tag{17}$$

where ϵ is Gaussian noise, and x, W, and y each follow a distribution. We embed the deviation term b in W. From a probabilistic view, once we know the distribution of W, through Equation (17) given the distribution of x, we obtain the distribution of y. The calculation is

$$\begin{aligned}p(y|X,w)&=\prod_{i=1}^{n}p\left(y_i|x_i,w\right)\\&=\prod_{i=1}^{n}\frac{1}{\sqrt{2\pi}\sigma_n}\exp\left(-\frac{\left(y_i-x_i^Tw\right)^2}{2\sigma_n^2}\right)\\&=\frac{1}{\left(2\pi\sigma_n^2\right)^{n/2}}\exp\left(-\frac{1}{2\sigma_n^2}\left|y-X^Tw\right|^2\right)\\&=\mathcal{N}\left(X^Tw,\sigma_n^2I\right).\end{aligned} \tag{18}$$

© Science China Press 2024

In a real-world scenario, however, it is difficult to obtain the distribution of W, under which the maximum posterior (MAP) method to estimate the posterior distribution of W has been proposed [179]. Once we have enough data pairs X,y to learn, the posterior will be infinitely close to the actual distribution of W. For this approach, we first give a simple Gaussian prior distribution to $W \sim \mathcal{N}(0, \sum_p)$ and then obtain from Bayes' rule that

$$p(w|X,y) = \frac{p(y|X,w)p(w)}{p(y|X)}, \tag{19}$$

where $p(y|X)$ is the marginal likelihood, which is a normalizing constant. Thus, the maximizing of the posterior distribution can be performed only with considering the likelihood and prior:

$$\begin{aligned} p(w|X,y) &\propto \exp\left(-\frac{1}{2\sigma_n^2}(y - X^T\omega)^T(y - X^T\omega)\right) \\ &\exp\left(-\frac{1}{2}w^T\Sigma_p^{-1}w\right) \\ &\propto \exp\left(-\frac{1}{2}(w-\overline{w})^T\left(\frac{1}{\sigma_n^2}XX^T + \Sigma_p^{-1}\right)(w-\overline{w})\right), \end{aligned} \tag{20}$$

where $\overline{w} = \sigma_n^{-2}\left(\sigma_n^{-2}XX^T + \Sigma_p^{-1}\right)^{-1}Xy$, and if we set $A = \sigma_n^{-2}XX^T + \Sigma_p^{-1}$, we find that the posterior distribution of W is a Gaussian distribution $p(w|X,y) \sim \mathcal{N}(\overline{w}, A^{-1})$. When a new sample $x_\star$ appears, its corresponding target value $y_\star$ follows the distribution of $\mathcal{N}\left(x_\star^T\overline{w}, x_\star^TA^{-1}x_\star\right)$. We usually choose the mean of this distribution as the final target value, and the covariance matrix describes the uncertainty in $y_\star$.

We use the kernel function to project the original sample feature into a high-dimensional space and thus increase the expressiveness of the Gaussian regression method. Richardson *et al.* [140] adopted GPR to estimate battery SOH, emphasizing the importance of choosing a proper kernel function. We denote the project function as $\phi(x)$ for one sample and $\Phi(X)$ for all samples in the training set. The basic regression formula Equation (17) is rewritten as

$$y = \phi(x)^TW + \epsilon. \tag{21}$$

We then abbreviate $\Phi(X)$ and $\phi(x_\star)$ as Φ and $\phi_\star$ respectively and substitute them into the predicted target distribution:

$$f_\star \mid x_\star, X, y \sim \mathcal{N}\left(\frac{1}{\sigma_n^2}\phi_\star^TA^{-1}\Phi y, \phi_\star^TA^{-1}\phi_\star\right). \tag{22}$$

In Equation (22), we need to calculate A^{-1}. When the dimensionality of A is large, the calculation time for this operation becomes unacceptable. We thus define $K = \Phi^T\sum_p\Phi$ and rewrite the above equation as

$$\begin{aligned} f_\star \mid x_\star, X, y &\sim \mathcal{N}(\phi_\star^T\sum_p\Phi\left(K + \sigma_n^2I\right)^{-1}y, \\ &\phi_\star^T\sum_p\phi_\star - \phi_\star^T\sum_p\Phi\left(K + \sigma_n^2I\right)^{-1}\Phi^T\sum_p\phi_\star. \end{aligned} \tag{23}$$

In this equation, we note that there are three similar terms, namely $\phi_\star^T\Sigma_p\Phi$,$\phi_\star^T\Sigma_p\phi_\star$ and $\Phi^T\Sigma_p\phi_\star$. Here, we choose $\phi(x)^T\Sigma_p\phi(x')$ as the example. This term is an inner product, Σ_p is positive definite, and we thus define $\left(\Sigma_p^{1/2}\right)^2 = \Sigma_p$ and $\psi(x) = \Sigma_p^{1/2}\phi(x)$. Finally, using Mercer's theorem, we get a new kernel function $k(x,x') = \psi(x)\psi(x')$ used in Equation (23). Liu *et al.* [180] demonstrated that GPR models that consider both electrochemical and empirical aging have distinct advantages in predicting battery capacity.

Regression tree

The regression tree is based on the decision tree method to make predictions, which offers a strong interpretable sense. Moreover, the aggregation of multiple decision trees can form an integrated learning model with excellent learning capability.

It can start with a classical regression tree method, namely the classification and regression tree (CART) [181]. Here, the decision tree comprises nodes and directed edges. There are two types of nodes, namely the internal node and leaf node, with the former representing a feature or an attribute, and the later for a class or value. When conducting a classification or regression task with a decision tree, the process starts from the root node, a feature of the sample is tested, and the sample is assigned to sub-nodes according to the test results. At this point, each sub-node corresponds to a value taken for that feature. The samples are tested and assigned in this way recursively until they reach the leaf nodes. In fact, the use of a decision tree is a way of dividing a space by a hyperplane. With each partitioning, the current space is divided according to the feature values, so that each leaf node is a disjoint region in the space. When the decision is made, the sample goes down step by step according to the value of each dimensional feature of the input sample. Finally, the sample falls into one of the N regions (assuming there are N leaf nodes).

Here, we give an example of CART used to predict a car price in Fig. 8b. We assume two features affect the price of a car, namely the horsepower and wheelbase, and the leaf node predicts the final price. Formally, we assume that X and Y are the input sample and corresponding target variables, respectively, and a training data set $D = (x_1,y_1),(x_2,y_2),\ldots,(x_N,y_N)$ is given. We now need to consider how to build a decision tree. A regression tree corresponds to a partition of the input space (i.e., feature space) and the output values on the partitioned cells. Suppose that the input space has been divided into M cells, $R_1,R_2,\ldots,R_M$, and each cell R_m has a fixed output value c_m. A regression tree model is represented as

$$f(x) = \sum_{m=1}^{M} c_mI(x \in R_m). \tag{24}$$

If the input space is already partitioned, the mean square error, $\sum_{x_i \in R_m}\left(y_i - f(x_i)\right)^2$, can be used to represent the prediction error, and the optimal value of each cell can be learned using this loss function. The optimal value $\widehat{c_m}$ on battery R_m should be the mean value of all output values y_i corresponding to cell R_m; i.e., $\widehat{c_m} = \text{mean}(y_i \mid x_i \in R_m)$.

Our consideration has two core problems, which are how to choose the division point and how to decide the output value of a leaf node in a tree. To solve the first question, the CART method adopts a heuristic approach to partition the input space

© Science China Press 2024

by selecting the $j-th$ variable $x^{(j)}$ and the value s as the splitting variable and the splitting point respectively, and then defines two regions:

$$R_1(j,s)=x\left|x^{(j)}\leqslant s\right\} \text{ and } R_2(j,s)=\left\{x\right|x^{(j)}>s. \quad (25)$$

The optimal division point is then found iteratively according to

$$\min_{j,s}\left[\min_{c_1}\sum_{x_i\in R_1(j,s)}(y_i-c_1)^2+\min_{c_2}\sum_{x_i\in R_2(j,s)}(y_i-c_2)^2\right]. \quad (26)$$

To solve the second issue, the selected optimal cut variable j and the optimal cut point s are used to partition the region and determine the corresponding output values:

$$\widehat{c_1}=\text{mean}\left(y_i|x_i\in R_1(j,s)\right) \text{and} \widehat{c_2}=\text{mean}\left(y_i|x_i\in R_2(j,s)\right)\Big\}. \quad (27)$$

We iterate through all input variables and find the optimal cut variable j, which forms a pair (j,s). In this way, the input space is divided into two regions. The above partitioning process is then repeated for each region until the stopping condition is satisfied. A regression tree is thus generated, which is usually called a least-squares regression tree.

Using a single regression tree is certainly not enough when dealing with specific practical problems. We can use the boosting framework in integrated learning to improve and upgrade the regression tree, and we refer to the new model as the boosting decision tree [182]. With further transformation, we get the gradient boosting decision tree [183], which can be further upgraded to XG-Boost [184] or light-GBM [185]. Yang *et al.* [186] proposed the gradient boosting regression tree (GBRT) model in 2020 to simulate the nonlinear degradation of batteries, obtaining an average error of approximately 7% in battery RUL prediction.

AR model

The regression method described in the previous section does not require temporal characteristics of the training data, such that the data can be collected at any time. However, such confusing temporal features sometimes cause problems in model learning. Suppose that we can use the data's temporal characteristics as learning parameters and continuously use the known sequence of data to predict the new data in the next moment. This further improves the model's estimation accuracy while reducing the model's learning difficulty. The problem of adding a temporal attribute to a dataset and predicting future arrivals from available data is called a time-series analysis problem. The autoregressive model is a basic method adopted to solve the time-series problem, as illustrated in Fig. 8c.

To begin, we assume any time-series data X_t can be represented by a weighted sum of historical data and a superposition of random perturbations:

$$X_t=a_1X_{t-1}+a_2X_{t-2}+\ldots+a_pX_{t-p}+\epsilon_t=\sum_{j=1}^{p}a_jX_t-j+\epsilon_t, \quad (28)$$

where a_j is a constant parameter, ϵ_t is the random perturbation, and our proposal is to find a suitable time-series $\{X_t\}$ for the given autoregressive model equation.

To calculate the solution to Equation (28), we need to know the backshift and linear constant coefficient difference equations. For any time-series $\{X_t\}$ and infinite series $\psi(z)=\sum_{j=-\infty}^{\infty}b_jz^j$, if $\sum_{j=-\infty}^{\infty}b_jX_{t-j}$ converges in a sense (i.e., convergence by probability, mean square convergence), we define

$$\psi(\mathcal{B})=\sum_{j=-\infty}^{\infty}b_j\mathcal{B}^j,$$
$$\psi(\mathcal{B})X_t=\sum_{j=-\infty}^{\infty}b_j\mathcal{B}^jX_t=\sum_{j=-\infty}^{\infty}b_jX_{t-j}. \quad (29)$$

$\mathcal{B}$ is the backshift operator at time t; obviously, we have $\mathcal{B}X_t=X_{t-j}$.

If $\{\epsilon_t\}$ is the white noise $\mathcal{N}\sim(0,\sigma^2)$, then Equation (28) becomes weakly stationary, and we can use the linear constant coefficient difference equation to solve this problem. This method is defined as follows. Given p real numbers $a_1,a_2,\ldots,a_p,a_p\neq0$,

$$X_t-\left[a_1X_{t-1}+a_2X_{t-2}+\ldots+a_pX_{t-p}\right]=0,t\neq Z, \quad (30)$$

which is called the rank p coefficient difference equation with a linear constant. The solution to Equation (30) is obtained using these p initial values $X_0,X_1,\ldots,X_{p-1}$. We introduce the backshift operator. We rewrite Equation (30) as $A(\mathcal{B})X_t=0,t\in Z$, and $A(z)=1-\sum_{j=1}^{p}a_jz^j$, where $A(z)$ is the characteristic polynomial of Equation (30). We now return to Equation (28). Based on the above fundamental concepts, we rewrite the equation as $A(\mathcal{B})X_t=\epsilon_t,t\in Z$. Letting the reciprocal roots of $A(z)$ be $z_1,z_2,\ldots,z_k$, for $1<\rho<\min\left\{\left|z_j\right|\right\}$, we have $A^{(-1)}(z)=1/A(z)$ as the analytic function of $\{z:|z|<\rho\}$, and we express A^{-1} as a Taylor series:

$$A^{-1}(z)=\sum_{j=0}^{\infty}\psi_jz^j,|z|\leqslant\rho, \quad (31)$$

We then substitute z for the backshift operator, and we obtain the stationary solution of Equation (28):

$$X_t=A^{-1}(\mathcal{B})\epsilon_t=\sum_{j=0}^{\infty}\psi_j\epsilon_{t-j},|t|\in Z. \quad (32)$$

Through the stochastic process calculation, we directly obtain the analytical solution of the whole series, and the model has strong interpretability and efficiency. However, the autoregressive model also has limitations in that it makes strong assumptions about the target time series, such as the weak stationary presumption, which is not satisfied by most time series in real scenarios. Therefore, to improve the model's generalization, many new methods have been explored to weaken the assumptions of the autoregressive model, such as the autoregressive moving average model [187], autoregressive integrated moving average (ARIMA) model [188], and vector autoregressive model [189]. Liu *et al.* [190] combined the autoregressive moving average model and KF for effective and robust estimation of battery SOC. Furthermore, Zhou and Huang [191] proposed a method based on the ARIMA model

 © Science China Press 2024

combined with empirical mode decomposition and found that it provided more accurate SOH estimation results than methods such as the RVM method.

FNN

ANNs are a series of mathematical models inspired by biology and neuroscience. These models simulate biological NNs by abstracting the neuronal network of the human brain, constructing artificial neurons, and establishing connections between artificial neurons according to a certain topology.

From the perspective of machine learning, an NN can generally be regarded as a nonlinear model, whose basic components are neurons with nonlinear activation functions. The connections among many neurons make the NN a highly nonlinear model. The weights of connections between neurons are the parameters that need to be learned and determined, which can be studied using gradient descent methods in the machine learning framework.

The feedforward NN (FNN) is one of the simplest NNs. Its structure is shown in Fig. 8d. For the regression scenario, we set $\mathbf{X} \in R^{n\times d}$ as n samples, each with d feature dimensions, and $\mathbf{O} \in R^{n}$ as the target values for the samples. For a single hidden-layer NN with h hidden units, the output of the hidden layer is represented as hidden representations. Both the hidden layer and output layer are fully connected, and we have the hidden-layer weights $\mathbf{W}^{(1)} \in R^{d\times h}$ and hidden-layer bias $\mathbf{b}^{(1)} \in R^{1\times h}$, and the output layer weights $\mathbf{W}^{(2)} \in R^{h\times 1}$ and the output-layer bias $\mathbf{b}^{(2)} \in R^{1\times 1}$. Formally, we compute the output of a single hidden-layer NN as

$$\begin{aligned}\mathbf{H} &= \mathbf{X}\mathbf{W}^{(1)} + \mathbf{b}^{(1)},\\ \mathbf{O} &= \mathbf{H}\mathbf{W}^{(2)} + \mathbf{b}^{(2)}.\end{aligned} \tag{33}$$

To fulfill the potential of the NN architecture, we need an additional key element: a nonlinear activation function σ applied to each hidden cell after the affine transformation. Such an activation function converts the linear model of Equation (33) into a nonlinear model with stronger representation capability:

$$\begin{aligned}\mathbf{H} &= \sigma(\mathbf{X}\mathbf{W}^{(1)} + \mathbf{b}^{(1)}),\\ \mathbf{O} &= \mathbf{H}\mathbf{W}^{(2)} + \mathbf{b}^{(2)}.\end{aligned} \tag{34}$$

To build a more general NN, we continue to stack such hidden layers, such as $\mathbf{H}^{(1)} = \sigma_1(\mathbf{X}\mathbf{W}^{(1)} + \mathbf{b}^{(1)})$ and $\mathbf{H}^{(2)} = \sigma_2(\mathbf{H}^{(1)}\mathbf{W}^{(2)} + \mathbf{b}^{(2)})$.

According to the universal approximation theorem [192], for an FNN with a linear output layer and at least one hidden layer, the squeezing property of the activation function can be used to approximate any bounded closed-set function defined in the real space R^D with arbitrary accuracy, as long as there are sufficient neurons in its hidden layer. Accordingly, each of the algorithms we mentioned earlier can theoretically be approximated by an NN to its model. However, such an NN has disadvantages: (1) the powerful fitting ability readily leads to model overfitting; (2) in achieving high accuracy, the model needs more training samples to determine many unknown parameters. Chen *et al.* [193] developed a method for estimating the battery SOC based on the FNN and EKF, confirming that the FNN is an effective method in practical and complex EV application environments.

RNN

The recurrent NN (RNN) is a deep learning method that considers time series data [194,195]. It combines the advantages of NN methods and time series methods. In an RNN, neurons receive information not only from other neurons but also from themselves, forming a network structure with loops. Compared with the FNN, the RNN is more in line with the structure of biological NNs.

The RNN processes temporal data of arbitrary length using neurons with self-feedback. Given an input time series $x_{1:T} = (x_1, x_2, \ldots, x_T)$, if we need to use information from time step $t-1$ to predict data of time step t, $P(x_t|x_{t-1}, \ldots, x_{t-n+1})$, we here learn a hidden state to represent the series information of time step $t-1$, i.e., namely $P(x_t|x_{t-1}, \ldots, x_{t-n+1}) \approx P(x_t|h_{t-1})$. In general, using the current input x_t and the previous hidden state h_{t-1} : $h_t = f(x_t, h_{t-1})$, we calculate the hidden state for any time at time step $t-1$. We then introduce the concept of the hidden state in the NN. We assume an n-sample series $\mathbf{X}_t \in R^{n\times d}$, where each row of $\mathbf{X}_t$ corresponds to one sample of time step t, and let $\mathbf{H}_t \in R^{n\times h}$ represent the hidden state of time step t. Unlike the FNN, we preserve the hidden state of the previous time step here, $\mathbf{H}_{t-1}$, and introduce a new weight parameter $\mathbf{W}_{hh} \in R^{h\times h}$ to describe how the hidden state of the previous time step is used in the current time step. Specifically, the hidden state of the current time step is calculated from the input of the current time step together with the hidden state of the previous time step:

$$\mathbf{H}_t = \phi(\mathbf{X}_t\mathbf{W}_{xh} + \mathbf{H}_{t-1}\mathbf{W}_{hh} + \mathbf{b}_h). \tag{35}$$

The relationship between the hidden state $\mathbf{H}_t$ and the adjacent time step $\mathbf{H}_{t-1}$ shows that these states capture and retain the history of the sequence up to the current time step, as the state or memory of the NN at the current time step, such that $\mathbf{H}_t$ is called the hidden state. The definition of the hidden state at the current time step is the same as the definition used in the previous time step, and the computation of Equation (35) is thus recurrent. Therefore, the recurrent-based hidden state NN is referred to as the RNN. The layer in the RNN that performs the computation of Equation (35) is called the recurrent layer.

For the final regression process, we design a special output layer:

$$\mathbf{O}_t = \mathbf{H}_t\mathbf{W}_{h1} + \mathbf{b}_1. \tag{36}$$

The parameters of the RNN include the weights $\mathbf{W}_{xh} \in R^{d\times h}, \mathbf{W}_{hh} \in R^{h\times h}$ and biases $\mathbf{b}_h \in R^{1\times h}$ of the hidden layer, and the weights $\mathbf{W}_{h1} \in R^{h\times 1}$ and biases $\mathbf{b}_1 \in R^{1\times 1}$ of the output layer. It is noted that the RNN uses these model parameters at different time steps. Therefore, the parameter overhead of the RNN does not increase as the number of time steps increases.

Fig. 8e illustrates the computational logic of the RNN at three adjacent time steps. At any time step, the computation of the hidden state can be considered as (1) splicing the input $\mathbf{X}_t$ of the current time step t with the hidden state $\mathbf{H}_{t-1}$ of the previous time step $t-1$ and (2) feeding the splicing result into a fully-connected layer with an activation function ϕ. The output of the fully connected layer is the hidden state $\mathbf{H}_t$ of the current time

© Science China Press 2024

step t. LSTM, which has become a research hotspot in recent years, can capture underlying long-term dependencies among the degraded capacities. Zhang *et al.* [196] used the LSTM-RNN method to estimate the battery RUL, which can be independent of offline data, and their experiments showed that the model had higher accuracy than the SVM and simple RNN. Table 2 lists the benefits and drawbacks of the proposed data-driven methods.

CNN

Convolutional NN (CNN) is a promising deep learning model for battery state estimation, which can autonomously learn data characteristics and efficiently process substantial volumes of data in a short duration, significantly accelerating battery detection and estimation. Additionally, its multi-layer architecture is adaptable to various types of battery data, serving as an excellent foundation for constructing the model with chemistry neutrality [197].

CNN has been widely used for feature extraction. A special type of CNN, namely multi-layer perceptron (MLP), is designed. The MLP structure can be divided into three layers: input layer, output layer, and hidden layer. The input layer is responsible for transferring the raw data to the first hidden layer. The output layer generates the desired output for the next program. The hidden layer consists of fully connected layers, max pooling layers, and convolutional layers. The convolutional layer is the primary building block of the CNN. It extracts local features from high-level inputs and passes all the information to lower levels to obtain more complex features. The output result vector o of the first convolutional layer can be represented by the following equation:

$$o_{ij}^{1} = \sigma\left(b_j^1 + \sum_{f_v=1}^{M} w_{f_{v,j}}^{1} x_{i+f_v-1,j}^{o}\right), \tag{37}$$

where σ, b_j, and w represents the sigmoid activation function, the bias for the j feature map, the weight of the kernel, respectively. f_v and x are the filter index and the power production input vector, respectively. Similarly, the outcome of the vector o output from the l convolutional layer can be expressed as follows:

$$o_{ij}^{l} = \sigma\left(b_j^l + \sum_{f_v=1}^{M} w_{f_{v,j}}^{l} x_{i+f_v-1,j}^{o}\right). \tag{38}$$

Max pooling layers are employed for dimensionality reduction, thereby further alleviating the computational burden of the model. The operation of the max pooling layer is given by the following expression:

$$p_{ij}^{l} = \max y_{i\times T+r,j}^{l-1} (r \in R), \tag{39}$$

where R represents the pooling size, T is the step size determining the distance for the input data area to be moved, which is smaller than the input dimension y. Fully connected layers connect every neuron in one layer to every neuron in the output layer.

In recent years, CNNs have been used for the analysis of time series data. For example, Shen *et al.* [198] used deep CNN (DCNN) to pre-train the data and integrated the resulting DCNN model with transfer learning techniques to estimate the capacity of commercial 18650 Li-ion batteries. The resulting root mean squared error (RMSE) and max error indicated that the proposed method outperforms other approaches such as the CNN with U-Net architecture (derived from fully CNN) proposed by Fan *et al.* [199] for SOC estimation, which achieved the accurate estimation with mean absolute error (MAE) less than 1.1% and RMSE less than 1.4% under constant temperature conditions. Wang *et al.* [200] introduced a closed-loop framework based on DCNN to capture the relationship between SOC and measurement equations of KF. The results demonstrate that the model exhibits excellent robustness and high accuracy, achieving an RMSE of less than 2.7%. However, it should be noted that CNN typically demands a substantial volume of training data. In the case of small sample datasets, CNN models are susceptible to overfitting, and their utilization entails extensive parameter tuning and high-end computing resources. Therefore, the application of CNN for battery estimation still encounters certain limitations.

Transformer model

The Transformer algorithm is a deep learning model employed for processing sequence data. By introducing an attention mechanism, the algorithm maps a query and a series of key-value pairs to an output, in which the sum of the weights on the value calculated according to the query and key is the output vector [201]. This can simultaneously learn varying attention weights, enabling it to focus on a broader range of information in the data. Transformer algorithm is very useful for processing long sequence data such as battery data. Moreover, this method can directly extract data features from raw data, significantly reducing the need for feature engineering. The general deep learning architecture is also well-suited to a wide range of battery types.

The transformer model is composed of stacked self-attention layers, encoders, decoders, and fully connected layers. This model has significantly transformed the implementation of attention mechanisms, relying solely on a self-attention mechanism constituted by scaled dot-product attention and multi-head attention. The scaled dot-product attention proposed by Vaswani *et al.* [202] firstly computes a dot product for each query, q, with all the keys, k. It subsequently divides each result by d_k and proceeds to apply a SoftMax function:

$$\text{Attention}(Q, K, V) = \text{softmax}\left(\frac{QK^T}{\sqrt{d_k}}\right)V. \tag{40}$$

The equation for the multi-head attention mechanism is predicated upon the forementioned scaled dot-product attention mechanism, as illustrated below:

$$\text{Multihead}(Q, K, V) = \text{Concat}(\text{head}_1, \ldots, \text{head}_n)W^o, \tag{41}$$

where each head_i, $i = 1, 2, \ldots, n$, implements a single attention function characterized by its own learned projection matrices as

$$\text{head}_i = \text{Attention}\left(QW_i^Q, KW_i^K, VW_i^V\right), \tag{42}$$

where q and k represent vectors of dimensions, and d_k contains the queries and keys, respectively. v denotes a vector of dimensions and d_v contains the values. Q, K, and V which denote matrices that pack together sets of queries, keys, and values, respectively. W^Q, W^K, and W^V enote projection matrices which are employed to generate different subspace representations of the query, key, and value matrices, respectively. W^O denotes a projection matrix for the multi-head output. Additionally, each

© Science China Press 2024

Table 2 Evaluation of data-driven methods

Method	Advantages	Disadvantages
LR	Simple regression model with low computational consumption; high generalizability	Weak representation; prone overfitting
RR	Able to handle many correlated features; reducing overfitting; low-complexity computation	Sensitive to hyperparameters; biased coefficients estimation; hard to get accurate standard errors
SVR	Self-prevention of overfitting or underfitting; able to deal with non-linear process	High-complexity computation; careful selection of function and decision of boundary distances highly required
GPR	Working well on small datasets; able to provide uncertainty measurements on the predictions	Hard to estimate the aleatoric uncertainty accurately with sparse data; hard to choose the window size for each dimension of input; high-complexity computation
RT	Handling non-linear parameters efficiently; no feature scaling required; feature preprocessing not required; easy to visualize; easy to understand	Not suitable for high-dimensional data; sensitive to outliers; weak generalization performance
AR	Better generations and more accurate likelihoods; not necessarily latent variable models; able to find recurring patterns in data, a small amount of data required	Slow in learning, inference, and generation; may introduce artificial bias when assumed order is imposed
FNN	Fixed computation time; high computation speed; learning general solutions of training data; no need an explicit model of a process	Large computational consumption, different types of architecture based on the data; easy to overfitting
RNN	Able to process inputs of any length; modeled to remember each information throughout the time; the fixed model size; able to process the arbitrary series of inputs	Slow computation; difficult to train the models; Prone to problems such as exploding and gradient vanishing

layer of the transformer's encoder and decoder contains a fully connected FNN, which is individually and uniformly applied at each positional index.

$$\mathrm{FFN}(x) = \max(0, xW_1 + b_1)W_2 + b_2. \tag{43}$$

Since the transformer model lacks recursion and convolution, "Positional Encoding" (PE) is applied to the input embeddings, encapsulating information regarding the relative or absolute positions of the tokens within a sequence.

$$\mathrm{PE}_{(\mathrm{pos},2i)} = \sin\left(\mathrm{pos}/10000^{2i/d_{\mathrm{model}}}\right), \tag{44}$$

$$\mathrm{PE}_{(\mathrm{pos},2i+1)} = \cos\left(\mathrm{pos}/10000^{2i+1/d_{\mathrm{model}}}\right), \tag{45}$$

where pos is the position and i represents the dimension.

The transformer method is now commonly used for feature extraction of battery. For example, Luo *et al.* [201] utilized a transformer-based NN to extract features from original battery data to estimate SOH. They achieved a mean absolute percentage error about 1.63% compared with the raw data. Additionally, the transformer method can be also combined with other deep learning methods to enhance the accuracy of battery states estimation. Li *et al.* [203] integrated the CNN and transformer learning to improve battery capacity estimation performance, demonstrating that this method can achieve fast online capacity estimation with high accuracy and computational efficiency. Similarly, Gu *et al.* [204] also employed a combination of CNN and transformer models to estimate battery SOH, achieving exceptional accuracy with the values of MAE, MAPE, and RMSE within the range of 0.55% for the NASA dataset. Nonetheless, similar to CNN, the transformer method also requires a significant amount of training data, and some large-scale transformer models may be too complex for certain battery estimation tasks, resulting in a lack of interpretability and overfitting.

PROSPECTS AND CONCLUSIONS

Challenges and prospects

Due to the environmentally friendly, long-lasting, and efficient properties, LIBs have achieved a significant level of commercial maturity and are expected to continue playing a critical role in EVs and energy storage systems. However, as shown in Fig. 9, the LIB ecosystem involves complex processes such as materials refinement, cell manufacturing, battery integration, application, and recycling. The collection and analysis of data are crucial for improving the safety and cost-effectiveness of LIBs. Nonetheless, challenges such as nonlinear degradation, state estimation, and failure warning continue to confront LIB applications. Thus, research on high-accuracy estimation of battery states such as SOC, SOH, and RUL is gaining increasing attention. Although considerable advancements have been achieved in battery states prognosis, it is important to note that ongoing research is still in its initial phases. The current focus remains primarily on nonlinear degradation and dynamic operational environments within practical applications. However, several challenges still need to be addressed, which can be broadly classified into two categories: forecasting methodology and real-world applications.

Regarding forecasting methods, there are two main challenges. Firstly, while attempting to incorporate multiple electrochemical properties and relevant parameters such as thermodynamic and mechanical parameters along with ambient temperature to improve accuracy, the resulting models often become complex, computationally intensive, and challenging to construct successfully. Secondly, relying solely on limited historical battery data without considering the degradation mechanism, such as

© Science China Press 2024

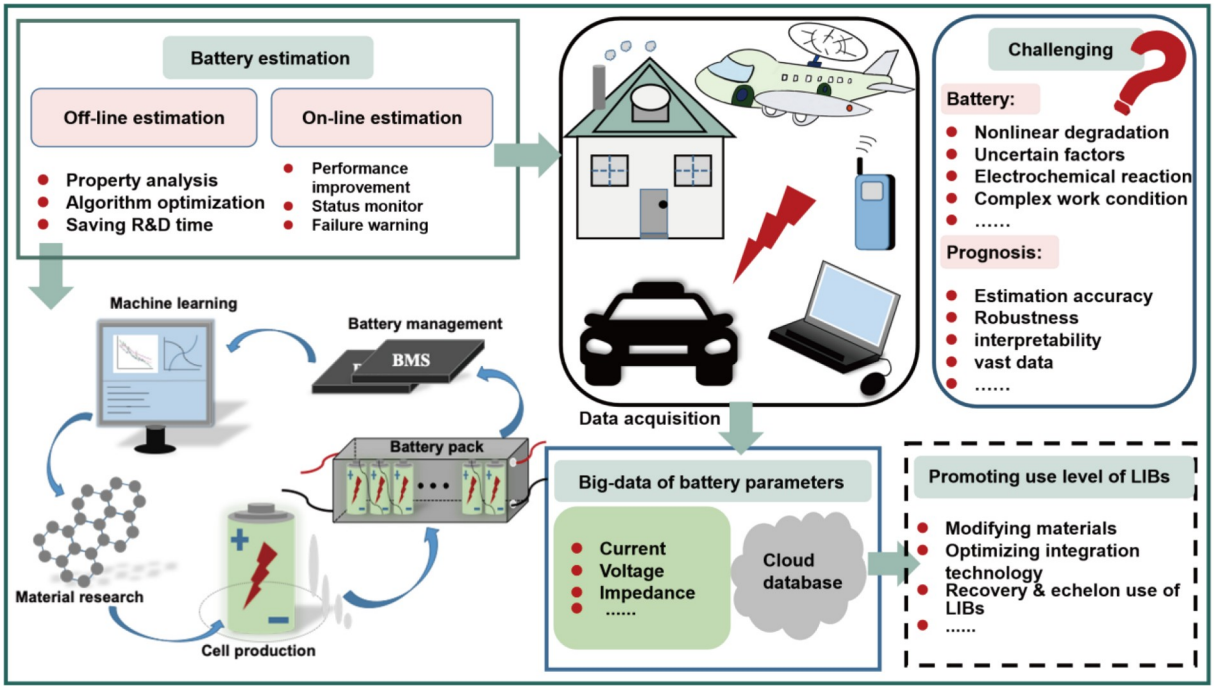

Figure 9 Battery application and challenge.

some machine learning technologies, renders the estimations less interpretable and offers little support for battery production and performance optimization. In terms of real-world applications, there are still significant obstacles to overcome. First, most existing studies on battery status estimation focus on a single type of battery, and the cycle dataset is collected within experimentally controlled environments, such as temperature, charge/discharge rate, and load. This setup makes it difficult to deploy the trained model in dynamic operating conditions and evolving environments in practical applications. Second, batteries are typically interconnected in parallel or series, forming a battery pack. This configuration introduces substantial variations in external conditions and operating environments compared with single cells studied, and obtaining experimental data for battery packs is more challenging.

Here, we have outlined several specific challenges that need to be addressed, which will also guide our future research efforts.

Development of hybrid methods with combination of EMs and machine learning

Firstly, to develop more accurate and explainable models for online estimation, it is crucial to implement the parameterization of EMs using simulation algorithms such as P2D, ECMs, and single particle models (SPM). These simulation algorithms allow for a comprehensive and systematic understanding of the internal reaction mechanisms, thus providing a theoretical basis for cell design and safety analysis. Additionally, combination machine learning methods with model parameterization can improve the accuracy and interpretability of battery estimation models [205]. Moreover, employing first-principles calculations together with the immense computational power also offers a promising approach. This method can consider various influencing parameters, including temperature, mechanical forces, electrochemical parameters, and thermodynamic parameters, to a greater extent than classical approaches, effectively enhancing the accuracy of battery status estimation [38]. For instance, Ming *et al.* [206] developed a model for predicting battery SOC using LSTM-NN, which considered dynamic stress, and achieved a maximum absolute error of only 2% during dynamic discharge. This demonstrates the feasibility and effectiveness of combining data-driven methods and first-principles calculation to predict the battery status.

Designing a model with chemistry neutrality

Development of a battery status prognosis model that is chemistry-neutral has emerged as a prominent trend in response to the limited reserves of traditional LIBs and the increasing demand of energy storage. This model aims to work with different cathode materials, including sodium, to overcome the limitations of conventional battery technologies. However, accurately estimating battery performance is influenced by both the electrode material and electrochemical properties, and most existing machine learning algorithms are tailored specifically for LIBs. Therefore, it is crucial to develop a predictive model that can accommodate various cathode materials and exhibit chemistry neutrality for accurate and versatile estimation.

Early prediction with reliable uncertainty-aware estimates

It is essential for accurately predicting the dynamic degradation process of batteries under various operating conditions. Developing a dependable prediction model that can accurately predict the whole degradation process, starting from any number of initial cycles, has become increasingly important for the recycling and cascade utilization of batteries. To ensure the accuracy and reliability of these predictions, implementing uncertainty-aware and explainable machine learning techniques is necessary. These techniques allow for the evaluation of prediction reliability and provide insight into the underlying factors affecting

© Science China Press 2024

battery performance.

Estimation battery performance under extreme conditions (temperature, pressure, etc.)

Most battery estimation models are constructed based on data collected in laboratory conditions, which typically involve room temperature and constant current or voltage profiles. However, battery degradation and internal reactions are influenced by various factors, especially temperature, which can significantly impact the aging mechanism of batteries, as discussed in section of "Aging mechanism". Developing a rapid estimation model that can cater to extreme conditions is essential for accurately evaluating battery performance and detecting online abnormalities. To achieve this, it is crucial to identify and extract effective aging features that are suitable for a broad range of conditions, and subsequently establish a machine learning algorithm capable of providing accurate estimations under these extreme operating scenarios.

Diagnosis of safety hazards

Efficiently diagnosing the battery fault is crucial due to the potential sudden and gradual failures during usage. Sudden failures pose a greater risk due to their shorter warning time, higher diagnostic difficulty, and potentially severe consequences, making it a challenging problem that requires immediate attention in the diagnosis of intrinsic battery failures. On the other hand, aging mechanisms in LIBs are complex, and there has been limited success in developing a quantitative evaluation of the degree of aging under multiple operating conditions, such as current, voltage, and temperature. Therefore, accurately diagnosing gradual failures is even more difficult than sudden failures, and requires further research to address this issue.

Estimation on the states of battery packs

In many applications, multiple batteries are integrated in series or parallel configurations to enhance power output or energy density. However, existing prediction models primarily focus on individual battery cells, which is inadequate when one cell within a battery pack becomes damaged or reaches its end-of-life (EOL), resulting in the deactivation of the entire pack. The incorporation of active or passive balancing technology modules within the battery pack helps adjust battery capacity, leading to varying degrees of capacity degradation and changes in impedance characteristics across different battery packs. Furthermore, when soft-pack batteries are utilized in battery packs, the limited space may restrict the swelling of battery cells, causing variations in the charge and discharge curve characteristics between the battery pack and independent battery cells. To address these challenges, the battery management field is witnessing a growing trend towards leveraging big data sharing platforms and information technology. These platforms enable the collection and exchange of diverse battery data, facilitating the development of more accurate, robust, and widely applicable estimation models.

CONCLUSIONS

This paper presents a comprehensive and systematic review of fundamental principles, current research progress, and degradation mechanisms of batteries, providing a thorough analysis of battery SOC, SOH, and RUL estimation methods. It sheds light on the foundational principles and specific implementation strategies of machine learning algorithms, thoroughly exploring the advantages and limitations of these methodologies. Furthermore, based on real-world scenarios, this paper suggests several innovative research directions that can serve as valuable references for researchers in the field of battery technology. Nevertheless, it is important to note that this paper only briefly touches on specific implementation steps, which may provide limited guidance for practical applications. Additionally, some prediction approaches do not consider battery pack configuration constraints, such as space limitations and load conditions. Therefore, further research is necessary to address these challenges and opportunities in the field of battery research.

Received 28 June 2023; accepted 25 October 2023; published online 19 February 2024

1 Lajunen A, Lipman T. Lifecycle cost assessment and carbon dioxide emissions of diesel, natural gas, hybrid electric, fuel cell hybrid and electric transit buses. Energy, 2016, 106: 329–342
2 Tarroja B, Zhang L, Wifvat V, *et al.* Assessing the stationary energy storage equivalency of vehicle-to-grid charging battery electric vehicles. Energy, 2016, 106: 673–690
3 Xiong R. Battery Management Algorithm for Electric Vehicles. Beijing: China Machine Press, 2020. 2–4
4 Deng D, Kim MG, Lee JY, *et al.* Green energy storage materials: Nanostructured TiO_2 and Sn-based anodes for lithium-ion batteries. Energy Environ Sci, 2009, 2: 818–837
5 Lai X, Jin C, Yi W, *et al.* Mechanism, modeling, detection, and prevention of the internal short circuit in lithium-ion batteries: Recent advances and perspectives. Energy Storage Mater, 2021, 35: 470–499
6 Tarascon JM, Armand M. Issues and challenges facing rechargeable lithium batteries. Nature, 2001, 414: 359–367
7 Nykvist B, Nilsson M. Rapidly falling costs of battery packs for electric vehicles. Nat Clim Change, 2015, 5: 329–332
8 Deng D. Li-ion batteries: Basics, progress, and challenges. Energy Sci Eng, 2015, 3: 385–418
9 Huang B, Pan Z, Su X, *et al.* Recycling of lithium-ion batteries: Recent advances and perspectives. J Power Sources, 2018, 399: 274–286
10 Nitta N, Wu F, Lee JT, *et al.* Li-ion battery materials: Present and future. Mater Today, 2015, 18: 252–264
11 Rezvanizaniani SM, Liu Z, Chen Y, *et al.* Review and recent advances in battery health monitoring and prognostics technologies for electric vehicle (EV) safety and mobility. J Power Sources, 2014, 256: 110–124
12 Dubarry M, Liaw BY. Identify capacity fading mechanism in a commercial $LiFePO_4$ cell. J Power Sources, 2009, 194: 541–549
13 Xu B, Oudalov A, Ulbig A, *et al.* Modeling of lithium-ion battery degradation for cell life assessment. IEEE Trans Smart Grid, 2018, 9: 1131–1140
14 Xiong R, Pan Y, Shen W, *et al.* Lithium-ion battery aging mechanisms and diagnosis method for automotive applications: Recent advances and perspectives. Renew Sustain Energy Rev, 2020, 131: 110048
15 Kassem M, Bernard J, Revel R, *et al.* Calendar aging of a graphite/$LiFePO_4$ cell. J Power Sources, 2012, 208: 296–305
16 Zhao R, Liu J, Gu J. A comprehensive study on Li-ion battery nail penetrations and the possible solutions. Energy, 2017, 123: 392–401
17 Broussely M, Biensan P, Bonhomme F, *et al.* Main aging mechanisms in Li ion batteries. J Power Sources, 2005, 146: 90–96
18 Xiong R, Yu Q, Wang LY, *et al.* A novel method to obtain the open circuit voltage for the state of charge of lithium ion batteries in electric vehicles by using H infinity filter. Appl Energy, 2017, 207: 346–353
19 Spotnitz R. Simulation of capacity fade in lithium-ion batteries. J Power Sources, 2003, 113: 72–80
20 Farmann A, Waag W, Marongiu A, *et al.* Critical review of on-board capacity estimation techniques for lithium-ion batteries in electric and hybrid electric vehicles. J Power Sources, 2015, 281: 114–130
21 Kan MS, Tan ACC, Mathew J. A review on prognostic techniques for non-stationary and non-linear rotating systems. Mech Syst Signal

 © Science China Press 2024

Proc, 2015, 62-63: 1–20
22 Lipu MSH, Hannan MA, Hussain A, *et al.* State of charge estimation for lithium-ion battery using recurrent NARX neural network model based lighting search algorithm. IEEE Access, 2018, 6: 28150–28161
23 Escobar LA, Meeker WQ. A review of accelerated test models. Statist Sci, 2006, 21: 552–577
24 Tian H, Qin P, Li K, *et al.* A review of the state of health for lithium-ion batteries: Research status and suggestions. J Cleaner Product, 2020, 261: 120813
25 Wang D, Miao Q, Pecht M. Prognostics of lithium-ion batteries based on relevance vectors and a conditional three-parameter capacity degradation model. J Power Sources, 2013, 239: 253–264
26 Wei J, Dong G, Chen Z. Remaining useful life prediction and state of health diagnosis for lithium-ion batteries using particle filter and support vector regression. IEEE Trans Ind Electron, 2017, 65: 5634–5643
27 Shen P, Ouyang M, Lu L, *et al.* The co-estimation of state of charge, state of health, and state of function for lithium-ion batteries in electric vehicles. IEEE Trans Veh Technol, 2017, 67: 92–103
28 Wang A, Zou Z, Wang D, *et al.* Identifying chemical factors affecting reaction kinetics in Li-air battery *via ab initio* calculations and machine learning. Energy Storage Mater, 2021, 35: 595–601
29 Zhao Q, Zhang L, He B, *et al.* Identifying descriptors for Li^+ conduction in cubic Li-argyrodites *via* hierarchically encoding crystal structure and inferring causality. Energy Storage Mater, 2021, 40: 386–393
30 Han X, Ouyang M, Lu L, *et al.* A comparative study of commercial lithium ion battery cycle life in electrical vehicle: Aging mechanism identification. J Power Sources, 2014, 251: 38–54
31 Gong C, Xue Z, Wen S, *et al.* Advanced carbon materials/olivine $LiFePO_4$ composites cathode for lithium ion batteries. J Power Sources, 2016, 318: 93–112
32 Li Y, Liu K, Foley AM, *et al.* Data-driven health estimation and lifetime prediction of lithium-ion batteries: A review. Renew Sustain Energy Rev, 2019, 113: 109254
33 Groot J. State-of-health Estimation of Li-ion Batteries: Cycle Life Test Methods. Sweden: Chalmers Tekniska Hogskola, 2012. 8–15
34 Cui Y, Du C, Yin G, *et al.* Multi-stress factor model for cycle lifetime prediction of lithium ion batteries with shallow-depth discharge. J Power Sources, 2015, 279: 123–132
35 Barré A, Deguilhem B, Grolleau S, *et al.* A review on lithium-ion battery ageing mechanisms and estimations for automotive applications. J Power Sources, 2013, 241: 680–689
36 Liu P, Wang J, Hicks-Garner J, *et al.* Aging mechanisms of $LiFePO_4$ batteries deduced by electrochemical and structural analyses. J Electrochem Soc, 2010, 157: A499
37 Xia ZY, Abu Qahouq JA. Adaptive and fast state of health estimation method for lithium-ion batteries using online complex impedance and artificial neural network. In: 2019 IEEE Applied Power Electronics Conference and Exposition (APEC). Anaheim: IEEE, 2019. 3361–3365
38 Hu X, Xu L, Lin X, *et al.* Battery lifetime prognostics. Joule, 2020, 4: 310–346
39 Dubarry M, Truchot C, Liaw BY. Synthesize battery degradation modes *via* a diagnostic and prognostic model. J Power Sources, 2012, 219: 204–216
40 Maher K, Yazami R. A study of lithium ion batteries cycle aging by thermodynamics techniques. J Power Sources, 2014, 247: 527–533
41 Harris SJ, Lu P. Effects of inhomogeneities—Nanoscale to mesoscale—On the durability of Li-ion batteries. J Phys Chem C, 2013, 117: 6481–6492
42 Joho F, Rykart B, Blome A, *et al.* Relation between surface properties, pore structure and first-cycle charge loss of graphite as negative electrode in lithium-ion batteries. J Power Sources, 2001, 97-98: 78–82
43 An SJ, Li J, Daniel C, *et al.* The state of understanding of the lithium-ion-battery graphite solid electrolyte interphase (SEI) and its relationship to formation cycling. Carbon, 2016, 105: 52–76
44 Cannarella J, Arnold CB. State of health and charge measurements in lithium-ion batteries using mechanical stress. J Power Sources, 2014, 269: 7–14
45 Ouyang CY, Zhong ZY, Lei MS. *Ab initio* studies of structural and electronic properties of $Li_4Ti_5O_{12}$ spinel. Electrochem Commun, 2007, 9: 1107–1112
46 Lu W, Liu J, Sun YK, *et al.* Electrochemical performance of $Li_{4/3}Ti_{5/3}O_4/Li_{1+x}(Ni_{1/3}Co_{1/3}Mn_{1/3})_{1-x}O_2$ cell for high power applications. J Power Sources, 2007, 167: 212–216
47 Shen X, Tian Z, Fan R, *et al.* Research progress on silicon/carbon composite anode materials for lithium-ion battery. J Energy Chem, 2018, 27: 1067–1090
48 Chung KY, Kim KB. Investigations into capacity fading as a result of a Jahn–Teller distortion in 4 V $LiMn_2O_4$ thin film electrodes. Electrochim Acta, 2004, 49: 3327–3337
49 Han X, Lu L, Zheng Y, *et al.* A review on the key issues of the lithium ion battery degradation among the whole life cycle. eTransportation, 2019, 1: 100005
50 Li X, Xu Y, Wang C. Suppression of Jahn–Teller distortion of spinel $LiMn_2O_4$ cathode. J Alloys Compd, 2009, 479: 310–313
51 Fleischhammer M, Waldmann T, Bisle G, *et al.* Interaction of cyclic ageing at high-rate and low temperatures and safety in lithium-ion batteries. J Power Sources, 2015, 274: 432–439
52 Jaguemont J, Boulon L, Dube Y. Characterization and modeling of a hybrid-electric-vehicle lithium-ion battery pack at low temperatures. IEEE Trans Veh Technol, 2015, 65: 1–14
53 Waldmann T, Wilka M, Kasper M, *et al.* Temperature dependent ageing mechanisms in Lithium-ion batteries—A Post-Mortem study. J Power Sources, 2014, 262: 129–135
54 Ouyang M, Ren D, Lu L, *et al.* Overcharge-induced capacity fading analysis for large format lithium-ion batteries with $Li_yNi_{1/3}Co_{1/3}Mn_{1/3}O_2 + Li_yMn_2O_4$ composite cathode. J Power Sources, 2015, 279: 626–635
55 Garche J, Jossen A, Döring H. The influence of different operating conditions, especially over-discharge, on the lifetime and performance of lead/acid batteries for photovoltaic systems. J Power Sources, 1997, 67: 201–212
56 Xiong R, Ma S, Li H, *et al.* Toward a safer battery management system: A critical review on diagnosis and prognosis of battery short circuit. iScience, 2020, 23: 101010
57 Ren D, Feng X, Lu L, *et al.* An electrochemical-thermal coupled overcharge-to-thermal-runaway model for lithium ion battery. J Power Sources, 2017, 364: 328–340
58 Yuan X, Liu H, Zhang J. Lithium-ion Batteries: Advanced Materials and Technologies. Boca Raton: CRC Press, 2011
59 Piller S, Perrin M, Jossen A. Methods for state-of-charge determination and their applications. J Power Sources, 2001, 96: 113–120
60 Li Z, Lu L, Ouyang M. Comparison of methods for improving SOC estimation accuracy through an ampere-hour integeration approach. Tsinghua Sci Technol, 2010, 50: 1293–1301
61 Zhang Y, Song W, Lin S, *et al.* A novel model of the initial state of charge estimation for $LiFePO_4$ batteries. J Power Sources, 2014, 248: 1028–1033
62 Liu X, Wu J, Zhang C, *et al.* A method for state of energy estimation of lithium-ion batteries at dynamic currents and temperatures. J Power Sources, 2014, 270: 151–157
63 Xiong R. Battery Management Algorithm for Electric Vehicle, Singapore: Springer, 2020.
64 Samad NA, Kim Y, Siegel JB, *et al.* Battery capacity fading estimation using a force-based incremental capacity analysis. J Electrochem Soc, 2016, 163: A1584–A1594
65 Feng X, Weng C, Ouyang M, *et al.* Online internal short circuit detection for a large format lithium ion battery. Appl Energy, 2016, 161: 168–180
66 How DNT, Hannan MA, Hossain Lipu MS, *et al.* State of charge estimation for lithium-ion batteries using model-based and data-driven methods: A review. IEEE Access, 2019, 7: 136116–136136
67 Tian J, Xiong R, Shen W. A review on state of health estimation for lithium ion batteries in photovoltaic systems. eTransportation, 2019, 2: 100028
68 Pop V, Bergveld HJ, Danilov D, *et al.* Battery Management Systems: Accurate State-of-charge Indication for Battery-powered Applications.

 © Science China Press 2024

Dordrecht: Springer, 2008. 24–37
69 Snihir I, Rey W, Verbitskiy E, *et al.* Battery open-circuit voltage estimation by a method of statistical analysis. J Power Sources, 2006, 159: 1484–1487
70 Sulzer V, Mohtat P, Lee S, *et al.* Promise and challenges of a data-driven approach for battery lifetime prognostics. In: 2021 American Control Conference (ACC). New Orleans: IEEE, 2021. 4427–4433
71 Severson KA, Attia PM, Jin N, *et al.* Data-driven prediction of battery cycle life before capacity degradation. Nat Energy, 2019, 4: 383–391
72 Roscher MA, Sauer DU. Dynamic electric behavior and open-circuit-voltage modeling of $LiFePO_4$-based lithium ion secondary batteries. J Power Sources, 2011, 196: 331–336
73 Dreyer W, Jamnik J, Guhlke C, *et al.* The thermodynamic origin of hysteresis in insertion batteries. Nat Mater, 2010, 9: 448–453
74 Blanke H, Bohlen O, Buller S, *et al.* Impedance measurements on lead-acid batteries for state-of-charge, state-of-health and cranking capability prognosis in electric and hybrid electric vehicles. J Power Sources, 2005, 144: 418–425
75 Zhang J, Lee J. A review on prognostics and health monitoring of Li-ion battery. J Power Sources, 2011, 196: 6007–6014
76 Zhang SS, Xu K, Jow TR. EIS study on the formation of solid electrolyte interface in Li-ion battery. Electrochim Acta, 2006, 51: 1636–1640
77 Roman D, Saxena S, Robu V, *et al.* Machine learning pipeline for battery state-of-health estimation. Nat Mach Intell, 2021, 3: 447–456
78 Holmström K, Petersson J. A review of the parameter estimation problem of fitting positive exponential sums to empirical data. Appl Math Computation, 2002, 126: 31–61
79 Doyle M, Fuller TF, Newman J. Modeling of galvanostatic charge and discharge of the lithium/polymer/insertion cell. J Electrochem Soc, 1993, 140: 1526–1533
80 Kroeze RC, Krein PT. Electrical battery model for use in dynamic electric vehicle simulations. In: 2008 IEEE Power Electronics Specialists Conference. Rhodes: IEEE, 2008. 1336–1342
81 He H, Xiong R, Guo H. Online estimation of model parameters and state-of-charge of $LiFePO_4$ batteries in electric vehicles. Appl Energy, 2012, 89: 413–420
82 Hu X, Li S, Peng H. A comparative study of equivalent circuit models for Li-ion batteries. J Power Sources, 2012, 198: 359–367
83 Freeborn TJ, Maundy B, Elwakil AS. Fractional-order models of supercapacitors, batteries and fuel cells: A survey. Mater Renew Sustain Energy, 2015, 4: 1–7
84 Yang Q, Xu J, Cao B, *et al.* A simplified fractional order impedance model and parameter identification method for lithium-ion batteries. PLoS ONE, 2017, 12: e0172424
85 Do DV, Forgez C, El Kadri Benkara K, *et al.* Impedance observer for a Li-ion battery using Kalman filter. IEEE Trans Veh Technol, 2009, 58: 3930–3937
86 Domenico DD, Fiengo G, Stefanopoulou A. Lithium-ion battery state of charge estimation with a Kalman filter based on a electrochemical model. In: 2008 IEEE International Conference on Control Applications. San Antonio: IEEE, 2019: 702–707
87 Kandepu R, Foss B, Imsland L. Applying the unscented Kalman filter for nonlinear state estimation. J Process Control, 2008, 18: 753–768
88 Li J, Klee Barillas J, Guenther C, *et al.* A comparative study of state of charge estimation algorithms for $LiFePO_4$ batteries used in electric vehicles. J Power Sources, 2013, 230: 244–250
89 Ristic B, Arulampalam S, Gordon N. Beyond the Kalman Filter: Particle Filters for Tracking Applications. Boston: Artech House, 2003. 830: 1–4
90 Plett GL. Extended Kalman filtering for battery management systems of LiPB-based HEV battery packs. J Power Sources, 2004, 134: 277–292
91 Junping W, Jingang G, Lei D. An adaptive Kalman filtering based state of charge combined estimator for electric vehicle battery pack. Energy Convers Manage, 2009, 50: 3182–3186
92 Mastali M, Vazquez-Arenas J, Fraser R, *et al.* Battery state of the charge estimation using Kalman filtering. J Power Sources, 2013, 239: 294–307
93 Xu L, Wang J, Chen Q. Kalman filtering state of charge estimation for battery management system based on a stochastic fuzzy neural network battery model. Energy Convers Manage, 2012, 53: 33–39
94 Yu Z, Huai R, Xiao L. State-of-charge estimation for lithium-ion batteries using a Kalman filter based on local linearization. Energies, 2015, 8: 7854–7873
95 Shrivastava P, Soon TK, Idris MYIB, *et al.* Overview of model-based online state-of-charge estimation using Kalman filter family for lithium-ion batteries. Renew Sustain Energy Rev, 2019, 113: 109233
96 Xiong R, Sun F, Chen Z, *et al.* A data-driven multi-scale extended Kalman filtering based parameter and state estimation approach of lithium-ion polymer battery in electric vehicles. Appl Energy, 2014, 113: 463–476
97 Xing Y, Ma EWM, Tsui KL, *et al.* An ensemble model for predicting the remaining useful performance of lithium-ion batteries. Microelectron Reliability, 2013, 53: 811–820
98 Gordon NJ, Salmond DJ, Smith AFM. Novel approach to nonlinear/non-Gaussian Bayesian state estimation. IEE Proc F Radar Signal Process UK, 1993, 140: 107
99 Wang Y, Zhang C, Chen Z. A method for state-of-charge estimation of $LiFePO_4$ batteries at dynamic currents and temperatures using particle filter. J Power Sources, 2015, 279: 306–311
100 Liu X, Chen Z, Zhang C, *et al.* A novel temperature-compensated model for power Li-ion batteries with dual-particle-filter state of charge estimation. Appl Energy, 2014, 123: 263–272
101 Merwe RVD, Doucet A, Freitas ND, *et al.* The unscented particle filter. In: Proceedings of the 13th International Conference on Neural Information Processing Systems. Cambridge: MIT Press, 2000. 1–7
102 Wang Y, Tian J, Sun Z, *et al.* A comprehensive review of battery modeling and state estimation approaches for advanced battery management systems. Renew Sustain Energy Rev, 2020, 131: 110015
103 Ungurean L, Cârstoiu G, Micea MV, *et al.* Battery state of health estimation: A structured review of models, methods and commercial devices. Int J Energy Res, 2017, 41: 151–181
104 Hatzell KB, Sharma A, Fathy HK. A survey of long-term health modeling, estimation, and control of lithium-ion batteries: Challenges and opportunities. In: 2012 American Control Conference (ACC). Montreal: IEEE, 2012. 584–591
105 Xiong R, Li L, Tian J. Towards a smarter battery management system: A critical review on battery state of health monitoring methods. J Power Sources, 2018, 405: 18–29
106 Berecibar M, Gandiaga I, Villarreal I, *et al.* Critical review of state of health estimation methods of Li-ion batteries for real applications. Renew Sustain Energy Rev, 2016, 56: 572–587
107 Ng KS, Moo CS, Chen YP, *et al.* Enhanced coulomb counting method for estimating state-of-charge and state-of-health of lithium-ion batteries. Appl Energy, 2009, 86: 1506–1511
108 Huet F. A review of impedance measurements for determination of the state-of-charge or state-of-health of secondary batteries. J Power Sources, 1998, 70: 59–69
109 Dai H, Wei X, Sun Z. A new SOH prediction concept for the power lithium-ion battery used on HEVs. In: 2009 IEEE Vehicle Power and Propulsion Conference. Dearborn: IEEE, 2012. 1649–1653
110 Waag W, Käbitz S, Sauer DU. Experimental investigation of the lithium-ion battery impedance characteristic at various conditions and aging states and its influence on the application. Appl Energy, 2013, 102: 885–897
111 Qahouq JAA, Xia Z. Single-perturbation-cycle online battery impedance spectrum measurement method with closed-loop control of power converter. IEEE Trans Ind Electron, 2017, 64: 7019–7029
112 Huang W, Qahouq JA. An online battery impedance measurement method using DC–DC power converter control. IEEE Trans Ind Electron, 2014, 61: 5987–5995
113 Pilla AA. A transient impedance technique for the study of electrode kinetics: Application to potentiostatic methods. J Electrochem Soc, 1970, 117: 467
114 Macdonald JR, Barsoukov E. Impedance Spectroscopy: Theory, Experiment, and Applications. Wiley-Interscience, Hoboken, 2018. 424–458

 © Science China Press 2024

115 Galeotti M, Cinà L, Giammanco C, *et al.* Performance analysis and SOH (state of health) evaluation of lithium polymer batteries through electrochemical impedance spectroscopy. Energy, 2015, 89: 678–686
116 Cui Y, Zuo P, Du C, *et al.* State of health diagnosis model for lithium ion batteries based on real-time impedance and open circuit voltage parameters identification method. Energy, 2018, 144: 647–656
117 Park C, Lahiri K, Raghunathan A. Battery discharge characteristics of wireless sensor nodes: An experimental analysis. In: 2005 Second Annual IEEE Communications Society Conference on Sensor and Ad Hoc Communications and Networks, 2005. IEEE SECON 2005. Santa Clara: IEEE, 2005. 430–440
118 Grillet AM, Humplik T, Stirrup EK, *et al.* The role of composite binder on mechanics and performance of lithium ion battery electrodes. Meet Abstr, 2016, MA2016-01: 368
119 Hardwick L, Buqa H, Novak P. Graphite surface disorder detection using *in situ* Raman microscopy. Solid State Ion, 2006, 177: 2801–2806
120 Finegan DP, Scheel M, Robinson JB, *et al. In-operando* high-speed tomography of lithium-ion batteries during thermal runaway. Nat Commun, 2015, 6: 6924
121 Schiffer ZJ, Cannarella J, Arnold CB. Strain derivatives for practical charge rate characterization of lithium ion electrodes. J Electrochem Soc, 2015, 163: A427–A433
122 Bloom I, Jansen AN, Abraham DP, *et al.* Differential voltage analyses of high-power, lithium-ion cells. J Power Sources, 2005, 139: 295–303
123 Weng C, Cui Y, Sun J, *et al.* On-board state of health monitoring of lithium-ion batteries using incremental capacity analysis with support vector regression. J Power Sources, 2013, 235: 36–44
124 Li Y, Abdel-Monem M, Gopalakrishnan R, *et al.* A quick on-line state of health estimation method for Li-ion battery with incremental capacity curves processed by Gaussian filter. J Power Sources, 2018, 373: 40–53
125 Merla Y, Wu B, Yufit V, *et al.* Novel application of differential thermal voltammetry as an in-depth state-of-health diagnosis method for lithium-ion batteries. J Power Sources, 2016, 307: 308–319
126 Lucu M, Martinez-Laserna E, Gandiaga I, *et al.* A critical review on self-adaptive Li-ion battery ageing models. J Power Sources, 2018, 401: 85–101
127 Dong H, Jin X, Lou Y, *et al.* Lithium-ion battery state of health monitoring and remaining useful life prediction based on support vector regression-particle filter. J Power Sources, 2014, 271: 114–123
128 Yu Q, Xiong R, Lin C, *et al.* Lithium-ion battery parameters and state-of-charge joint estimation based on H-infinity and unscented Kalman filters. IEEE Trans Veh Technol, 2017, 66: 8693–8701
129 Wei Z, Zhao J, Ji D, *et al.* A multi-timescale estimator for battery state of charge and capacity dual estimation based on an online identified model. Appl Energy, 2017, 204: 1264–1274
130 Bose CSC, Laman FC. Battery state of health estimation through coup de fouet. In: INTELEC. Twenty-Second International Telecommunications Energy Conference (Cat. No.00CH37131). Phoenix: IEEE, 2000. 597–601
131 Chen C, Pecht M. Prognostics of lithium-ion batteries using model-based and data-driven methods. In: Proceedings of the IEEE 2012 Prognostics and System Health Management Conference (PHM-2012 Beijing). Beijing: IEEE, 2012. 1–6
132 Wu L, Fu X, Guan Y. Review of the remaining useful life prognostics of vehicle lithium-ion batteries using data-driven methodologies. Appl Sci, 2016, 6: 166
133 Lipu MSH, Hannan MA, Hussain A, *et al.* A review of state of health and remaining useful life estimation methods for lithium-ion battery in electric vehicles: Challenges and recommendations. J Cleaner Product, 2018, 205: 115–133
134 Saha B, Poll S, Goebel K, *et al.* An integrated approach to battery health monitoring using bayesian regression and state estimation. In: 2007 IEEE Autotestcon. Baltimore: IEEE, 2007. 646–653
135 Zou Y, Hu X, Ma H, *et al.* Combined state of charge and state of health estimation over lithium-ion battery cell cycle lifespan for electric vehicles. J Power Sources, 2015, 273: 793–803
136 Xiong R, Zhang Y, He H, *et al.* A double-scale, particle-filtering, energy state prediction algorithm for lithium-ion batteries. IEEE Trans Ind Electron, 2017, 65: 1526–1538
137 Hu C, Jain G, Schmidt C, *et al.* Online estimation of lithium-ion battery capacity using sparse Bayesian learning. J Power Sources, 2015, 289: 105–113
138 Ng SSY, Xing Y, Tsui KL. A naive Bayes model for robust remaining useful life prediction of lithium-ion battery. Appl Energy, 2014, 118: 114–123
139 Yang F, Wang D, Xing Y, *et al.* Prognostics of Li(NiMnCo)O_2-based lithium-ion batteries using a novel battery degradation model. Microelectron Reliability, 2017, 70: 70–78
140 Richardson RR, Osborne MA, Howey DA. Gaussian process regression for forecasting battery state of health. J Power Sources, 2017, 357: 209–219
141 Rasmussen CE. Gaussian processes in machine learning. Springer, 2003. 63–71
142 Ažman K, Kocijan J. Dynamical systems identification using Gaussian process models with incorporated local models. Eng Appl Artif Intelligence, 2011, 24: 398–408
143 Tang S, Yu C, Wang X, *et al.* Remaining useful life prediction of lithium-ion batteries based on the wiener process with measurement error. Energies, 2014, 7: 520–547
144 Sahinoglu GO, Pajovic M, Sahinoglu Z, *et al.* Battery state-of-charge estimation based on regular/recurrent Gaussian process regression. IEEE Trans Ind Electron, 2017, 65: 4311–4321
145 Williams C, Rasmussen C. Gaussian processes for regression. In: Proceedings of the 8th International Conference on Neural Information Processing Systems. Cambridge: MIT Press, 1995. 8: 514–520
146 Ebden M. Gaussian processes: A quick introduction, arXiv: 2015.02965
147 Liu D, Pang J, Zhou J, *et al.* Prognostics for state of health estimation of lithium-ion batteries based on combination Gaussian process functional regression. Microelectron Reliability, 2013, 53: 832–839
148 Chen Z, Mi CC, Fu Y, *et al.* Online battery state of health estimation based on Genetic Algorithm for electric and hybrid vehicle applications. J Power Sources, 2013, 240: 184–192
149 Nuhic A, Terzimehic T, Soczka-Guth T, *et al.* Health diagnosis and remaining useful life prognostics of lithium-ion batteries using data-driven methods. J Power Sources, 2013, 239: 680–688
150 Sankavaram C, Pattipati B, Kodali A, *et al.* Model-based and data-driven prognosis of automotive and electronic systems. In: 2009 IEEE International Conference on Automation Science and Engineering. Bangalore: IEEE, 2009. 96–101
151 Kulkarni C, Biswas G, Saha S, *et al.* A model-based prognostics methodology for electrolytic capacitors based on electrical overstress accelerated aging. In: Annual Conference of the Prognostics and Health Management Society. Montreal, 2011. 3: 1–9
152 Shi S, Gao J, Liu Y, *et al.* Multi-scale computation methods: Their applications in lithium-ion battery research and development. Chin Phys B, 2015, 25: 018212
153 Beale MH, Hagan MT, Demuth HB. Neural Network Toolbox. Natick: The MathWorks, 2010. 2: 77–81
154 Hagan MT, Demuth HB, Beale MH. Neural Network Design. Boston: PWS Publishing Co., 1997. 22–23
155 Andre D, Nuhic A, Soczka-Guth T, *et al.* Comparative study of a structured neural network and an extended Kalman filter for state of health determination of lithium-ion batteries in hybrid electricvehicles. Eng Appl Artif Intelligence, 2013, 26: 951–961
156 Widodo A, Shim MC, Caesarendra W, *et al.* Intelligent prognostics for battery health monitoring based on sample entropy. Expert Syst Appl, 2011, 38: 11763–11769
157 Cheng D, Sha W, Wang L, *et al.* Solid-state lithium battery cycle life prediction using machine learning. Appl Sci, 2021, 11: 4671
158 Lombardo T, Duquesnoy M, El-Bouysidy H, *et al.* Artificial intelligence applied to battery research: Hype or reality? Chem Rev, 2022, 122: 10899–10969
159 Saha KGB. Battery Data Set, NASA Ames Prognostics Data Repository 2007. http://ti.arc.nasa.gov/project/prognostic-datarepository
160 Ni Y, Xu J, Zhu C, *et al.* Accurate residual capacity estimation of retired $LiFePO_4$ batteries based on mechanism and data-driven model.

 © Science China Press 2024

Appl Energy, 2022, 305: 117922
161 Liu Y, Yang Z, Yu Z, *et al.* Generative artificial intelligence and its applications in materials science: Current situation and future perspectives. J Materiomics, 2023, 9: 798–816
162 Liu Y, Yang Z, Zou X, *et al.* Data quantity governance for machine learning in materials science. Natl Sci Rev, 2023, 10: 125
163 Liu Y, Wang S, Yang Z, *et al.* Auto-matRegressor: Liberating machine learning alchemists. Sci Bull, 2023, 68: 1259–1270
164 Poole MA, O'Farrell PN. The assumptions of the linear regression model. Trans Institute Br Geographers, 1971, 52: 145–158
165 Seber GA, Lee AJ. Linear Regression Analysis. Hoboken: John Wiley & Sons, 2012. 2: 1–20
166 Vilsen SB, Stroe DI. Battery state-of-health modelling by multiple linear regression. J Cleaner Product, 2021, 290: 125700
167 Hong J, Wang Z, Chen W, *et al.* Online joint-prediction of multi-forward-step battery SOC using LSTM neural networks and multiple linear regression for real-world electric vehicles. J Energy Storage, 2020, 30: 101459
168 Hoerl AE, Kennard RW. Ridge regression: Biased estimation for nonorthogonal problems. Technometrics, 1970, 12: 55–67
169 Tibshirani R. Regression shrinkage and selection *via* the lasso. J R Stat Soc B, 1996, 58: 267–288
170 Wu J, Cui X, Zhang H, *et al.* Health prognosis with optimized feature selection for lithium-ion battery in electric vehicle applications. IEEE Trans Power Electron, 2021, 36: 12646–12655
171 Jiang Y, Jiang J, Zhang C, *et al.* State of health estimation of second-life $LiFePO_4$ batteries for energy storage applications. J Cleaner Product, 2018, 205: 754–762
172 Lin D, Zhang Y, Zhao X, *et al.* Early prediction of remaining useful life for grid-scale battery energy storage system. J Energy Eng, 2021, 147: 04021046
173 Drucker H, Burges CJ, Kaufman L, *et al.* Support vector regression machines. In: Proceedings of Advances in Neural Information Processing Systems 9. Cambridge: MIT Press 1996. 155–161
174 Boyd SP, Vandenberghe L. Convex Optimization. Los Angeles: Cambridge University Press, 2004, 12–108
175 Platt J. Sequential minimal optimization: A fast algorithm for training support vector machines. Microsoft, 1998, 14: 7–9
176 Cortes C, Vapnik V. Support-vector networks. Mach Learn, 1995, 20: 273–297
177 Li R, Xu S, Li S, *et al.* State of charge prediction algorithm of lithium-ion battery based on PSO-SVR cross validation. IEEE Access, 2020, 8: 10234–10242
178 Mercer J. Functions of positive and negative type and their commection with the theory of integral equations. Philos Trinsdictions Rogyal Soc, 1909, 209: 4–415
179 Abdolmaleki A, Springenberg JT, Tassa Y, *et al.* Maximum a posteriori policy optimisation, arXiv: 1806.06920
180 Liu K, Hu X, Wei Z, *et al.* Modified gaussian process regression models for cyclic capacity prediction of lithium-ion batteries. IEEE Trans Transp Electrific, 2019, 5: 1225–1236
181 Breiman L. Classification and Regression Trees. New York: Routledge, 2017. 1–14
182 Freund Y, Mason L. The alternating decision tree learning algorithm. In: Proceedings of the Sixteenth International Conference on Machine Learning. San Francisco: Morgan Kaufmann Publishers Inc., 1999. 124–133
183 Friedman JH. Stochastic gradient boosting. Comput Stat Data Anal, 2002, 38: 367–378
184 Chen T, Guestrin C. Xgboost: A scalable tree boosting system. In: Proceedings of the 22nd ACM SIGKDD International Conference on Knowledge Discovery and Data Mining. New York: Association for Computing Machinery, 2016. 785–794
185 Ke G, Meng Q, Finley T, *et al.* Lightgbm: A highly efficient gradient boosting decision tree. In: Proceedings of the 31st International Conference on Neural Information Processing Systems. Red Hook: Curran Associates Inc., 2017. 1–8
186 Yang F, Wang D, Xu F, *et al.* Lifespan prediction of lithium-ion batteries based on various extracted features and gradient boosting regression tree model. J Power Sources, 2020, 476: 228654
187 Box GEP, Jenkins GM, Reinsel GC, *et al.* Time series analysis: Forecasting and control. Oper Res-Ger, 2015, 22: 199–201
188 Nelson BK. Time series analysis using autoregressive integrated moving average (ARIMA) models. Acad Emerg Med, 1998, 5: 739–744
189 Lütkepohl H. Vector Autoregressive Models. Cheltenham: Edward Elgar Publishing, 2013. 6: 139–164
190 Liu Z, Dang X, Jing B, *et al.* A novel model-based state of charge estimation for lithium-ion battery using adaptive robust iterative cubature Kalman filter. Electric Power Syst Res, 2019, 177: 105951
191 Zhou Y, Huang M. Lithium-ion batteries remaining useful life prediction based on a mixture of empirical mode decomposition and ARIMA model. Microelectron Reliability, 2016, 65: 265–273
192 Cybenko G. Approximation by superpositions of a sigmoidal function. Math Control Signal Syst, 1989, 2: 303–314
193 Chen C, Xiong R, Yang R, *et al.* State-of-charge estimation of lithium-ion battery using an improved neural network model and extended Kalman filter. J Cleaner Product, 2019, 234: 1153–1164
194 Rumelhart DE, Hinton GE, Williams RJ. Learning representations by back-propagating errors. Nature, 1986, 323: 533–536
195 Hochreiter S, Schmidhuber J. Long short-term memory. Neural Comput, 1997, 9: 1735–1780
196 Zhang Y, Xiong R, He H, *et al.* Long short-term memory recurrent neural network for remaining useful life prediction of lithium-ion batteries. IEEE Trans Veh Technol, 2018, 67: 5695–5705
197 Liu Y, He Y, Bian H, *et al.* A review of lithium-ion battery state of charge estimation based on deep learning: Directions for improvement and future trends. J Energy Storage, 2022, 52: 104664
198 Shen S, Sadoughi M, Li M, *et al.* Deep convolutional neural networks with ensemble learning and transfer learning for capacity estimation of lithium-ion batteries. Appl Energy, 2020, 260: 114296
199 Fan X, Zhang W, Zhang C, *et al.* SOC estimation of Li-ion battery using convolutional neural network with U-Net architecture. Energy, 2022, 256: 124612
200 Wang Q, Ye M, Wei M, *et al.* Deep convolutional neural network based closed-loop SOC estimation for lithium-ion batteries in hierarchical scenarios. Energy, 2023, 263: 125718
201 Luo K, Zheng H, Shi Z. A simple feature extraction method for estimating the whole life cycle state of health of lithium-ion batteries using transformer-based neural network. J Power Sources, 2023, 576: 233139
202 Vaswani A, Shazeer N, Parmar N, et al. Attention is all you need. In: Proceedings ofthe 31st International Conference on Neural Information Processing Systems. Red Hook: Curran Associates Inc., 2017. 30.
203 Li Y, Li K, Liu X, *et al.* Lithium-ion battery capacity estimation—A pruned convolutional neural network approach assisted with transfer learning. Appl Energy, 2021, 285: 116410
204 Gu X, See KW, Li P, *et al.* A novel state-of-health estimation for the lithium-ion battery using a convolutional neural network and transformer model. Energy, 2023, 262: 125501
205 Zhao Q, Avdeev M, Chen L, *et al.* Machine learning prediction of activation energy in cubic Li-argyrodites with hierarchically encoding crystal structure-based (HECS) descriptors. Sci Bull, 2021, 66: 1401–1408
206 Ming T, Wang K, Tian D. Estimation on state of charge of lithium battery based on lstm neural network. Guangdong Electric Power, 2020, 33: 26–33

Acknowledgements This work was supported by the major program funds of State Grid Shaanxi Electric Power Company Limited (5226KY23000P) and the Startup funds of Yangtze Delta Region Institute (Huzhou), University of Electronic Science and Technology of China (U03210019).

Author contributions Yuan J, Huang H, Liu S and Sun C wrote the section of AGING MECHANISM AND INFLUENCING FACTORS. Yuan J, Huang H, Gan X, Liu S and Bi C wrote the section of TRADITIONAL TECHNOLOGIES FOR SOC, SOH AND RUL ESTIMATION. Qin Z, Wang Z, Yang Y and Wen A wrote the section of MACHINE LEARNING METHODS

 © Science China Press 2024

FOR SOC, SOH AND RUL ESTIMATION. Li B and Sun C supervised the project, wrote the INTRODUCTION and section of PROSPECTS AND CONCLUSIONS. All authors contributed to the general discussion and revised the manuscript.

Conflict of interest The authors declare that they have no conflict of interest.

Jun Yuan received her Bachelor's degree in materials science and engineering from Chengdu University of Technology and Master's degree in materials science and engineering from the University of Electronic Science and Technology of China (UESTC) in 2023. She is currently working toward her PhD degree in digital catalysis at the Department of Chemistry, Technical University of Munich in Germany. Her research interests include battery states estimation and early faulty diagnosis using machine learning and electrochemical models.

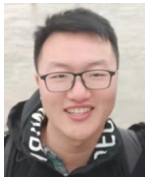

Zhili Qin received his Bachelor's degree in computer science from Hefei University of Technology in 2017. He is currently pursuing his PhD degree at UESTC. In 2022, he participated in a one-year academic exchange program supported by China Scholarship Council (CSC) Scholarship at Ludwig Maximilian University of Munich in Germany. His primary research interests focus on the areas of multi-label learning, few-shot learning, and zero-shot learning, etc.

Baihai Li received his PhD degree from the Chinese Academy of Sciences in 2011 and subsequently served as a postdoctoral fellow at the University of Michigan-Ann Arbor. In 2013, Dr. Li joined the School of Materials and Energy, UESTC as an associate professor. His research primarily focuses on energy conversion and storage, especially for battery material surfaces/interfaces and intelligent battery management, such as data-driven estimation of battery states and early faulty diagnosis, employing a combination of machine learning techniques and electrochemical models.

Chenghua Sun received his PhD degree from the Chinese Academy of Sciences in 2007 and then joined the University of Queensland (Brisbane, Australia) as a postdoc fellow. In 2013, Dr. Sun joined the School of Chemistry, Monash University as a lecturer and established his group on computer-aided catalyst design. He was awarded ARC Future Fellow and joined the Swinburne University of Technology in 2017 as an associate professor. His research focuses on catalyst design for clean energy and environment applications, particularly for ammonia synthesis, methane combustion, batteries, and biomass conversion.

电池衰减诊断及状态评估研究进展

袁君[1,2†], 秦之理[2,3†], 黄海坤[1,2], 甘兴栋[1,2], 王子为[4], 杨毅琛[4], 刘书江[1,2], 文安[2], 毕闯[2], 李白海[1,2*], 孙成华[5*]

摘要 锂离子电池(LIB)广泛应用于储能及动力输出等领域. 准确预测电池的健康状态对于优化性能、降低运营费用和防止电池故障等方面具有重要的意义. 本文对预测LIB的荷电状态(SOC)、健康状态(SOH)和剩余使用寿命(RUL)方面的最新发展进行了全面回顾, 重点关注机器学习技术方面的研究进展, 深入分析了LIB的退化机制及其基本理论, 评估了各种传统方法及机器学习技术在预测SOC, SOH和RUL方面的优势和限制. 此外, 还探讨了电动汽车动力电池在实际应用中面临的挑战, 特别是性能退化问题.最后提出了对LIB未来研究方向有价值的见解. 尽管机器学习方法在提高预测SOC, SOH和RUL准确性方面具有巨大潜力, 但在实际应用中仍然有许多技术和实际障碍需要克服.

© Science China Press 2024